Topographic and Faults Control of Hydrothermal Circulation Along Dormant Faults in an Orogen

Audrey Taillefer, Laurent Guillou-Frottier, Roger Soliva, Fabien Magri, Simon Lopez, Gabriel Courrioux, Romain Millot, Bernard Ladouche, Elisabeth Le Goff

Topographic and faults control of hydrothermal circulation along dormant faults in an orogen.

Audrey Taillefer[1], Laurent Guillou-Frottier[2,3], Roger Soliva[1], Fabien Magri[4,5], Simon Lopez[2], Gabriel Courrioux[2], Romain Millot[2], Bernard Ladouche[6], Elisabeth Le Goff[6]

[1] Géosciences Montpellier, University of Montpellier, F-34095, France.

[2] BRGM, F-45060 Orléans, France.

[3] ISTO, UMR 7327, Université d'Orléans, CNRS, BRGM, F-45071 Orléans, France.

[4] Helmholtz-Zentrum für Umweltforschung GmbH – UFZ, Leipzig, Germany.

[5] Freie Universität Berlin, 12249 Berlin, Germany.

[6] BRGM, F-34000, Montpellier, France.

Corresponding author: Laurent Guillou-Frottier (l.guillou-frottier@brgm.fr)

Key Points:

- 3-D numerical models of the Têt hydrothermal system (Eastern Pyrénées, France) constrained by structural field data and hydrochemistry.
- Impacts of a complex 3-D topography on the location of hot springs.
- Impacts of a dormant fault network and its permeability on hot spring temperatures (29-73°C).

This article has been accepted for publication and undergone full peer review but has not been through the copyediting, typesetting, pagination and proofreading process which may lead to differences between this version and the Version of Record. Please cite this article as doi: 10.1029/2018GC007965

Abstract

Hydrothermal systems involving dormant faults within orogenic belts are rarely targeted for geothermal exploration, partly because of the complexity of the 3-D topography, the unknown permeability of the fault zones and the basement lithology, and the lack of deep-level data. This study brings together various types of surface information (spring features, geological data, topography, hydrochemistry) to explain the alignment of 29 hot springs (29-73°C) along the dormant Têt fault (Eastern Pyrénées, France). Water ion concentrations, stable water isotopes and lithium isotopic ratios indicate that (i) fluids originating from meteoric water infiltrate above an altitude of 2000 m, (ii) the rocks interacting with the fluids are similar for all the springs, and (iii) the maximum fluid temperatures at depth show similar variations along the fault and at the surface. A 3-D numerical model of the system, assembled from field structural data and from a Digital Elevation Model, explores the permeability combinations for the basement and for a three-fault network. The models indicate that for a relatively permeable basement (10^{-16} m^2), fluids are topography-driven down to thousands of meters (until -3700 m) before being captured by the more permeable Têt fault. Hot spring temperatures can be numerically reproduced when fault permeability is around 10^{-14} m^2, a value slightly lower than the critical permeability for which free-convection would occur within the Têt fault. Our study shows that thermal anomalies are possible along dormant faults close to elevated topography in the core of an orogenic belt, thereby opening new perspectives for geothermal exploration.

Plain language summary

The occurrence of hot springs around the world is not easy to explain in place where there are no volcanoes to heat water in the ground, e.g., in Iceland. These hot springs are commonly encountered in the vicinity of seismic faults, which are crushed rocks acting as pipes driving water within the crust. The rocks at deep levels are naturally hot and heat water that will supply the hot springs at the surface.

In the mountain range of Pyrénées (South of France), 29 hot springs with temperatures ranging between 29 and 73°C are observed along the Têt fault. That fault does not record significant seismic activity since 5 Ma, suggesting that the pipe is likely clogged. In this study, we used chemical analyses of the hydrothermal water, field data of the topography, the hot springs, the faults, fractures and rocks, to understand the functioning of this hydrothermal system. We also reproduced the fluid circulations in a 3-D numerical model of the study area.

We show that fluids originate from the infiltration of rainwater in the highlands. The high topography controls the circulation of fluids in the crust (until -3700m), hence the hot springs location at the surface. The Têt fault is still acting as pipe from deep levels to the surface, allowing the fast ascension of the hot fluids (until 130°C for the hottest) that allows them to not become cold. These hydrothermal systems are commonly encountered within continents, and could be a great source of renewable energy to produce electricity (i.e., the geothermic energy).

1 Introduction

Continental hydrothermal systems without magmatic heat sources are currently targeted for the production of high-temperature geothermal energy, as in the Basin and Range

Province, USA (e.g. Blackwell et al., 2000; Faulds et al., 2010) or in western Anatolia Turkey (Roche et al., 2018). In these systems, meteoric waters infiltrate at high altitude, flow down into the shallow crust where they are warmed by the increasing natural temperature, and then seek pathways to quickly reach the surface before losing heat (Grasby and Hutcheon, 2001; Mckenna and Blackwell, 2004; Craw et al., 2013). Studies commonly focus on active extensional contexts (e.g., Dixie Valley, Nevada) where the normal fault offsets induce high symmetrical, cylindrical and smooth topography associated with high permeabilities both in the fault zones and in sedimentary basins, or along highly active faults where frictional heating and transport of warm rocks from depth are common (e.g. Saffer et al., 2003; Cox et al., 2015; Sutherland et al., 2017). However, it has recently been suggested that strong geothermal anomalies may also form along dormant faults (i.e., low current seismicity Mw < 4 and small cumulated offsets of < 300m during the last 10 Ma) close to high topography in the core of an *orogenic belt context* as defined by Moeck, 2014 (e.g. Grasby and Hutcheon, 2001; Allen et al., 2006; Ge et al., 2008; Thiebaud, 2008, Thiebaud et al., 2010; Craw et al., 2013; Taillefer et al., 2017).

Because these environments are rarely targeted for oil or mining exploration, and because of the limited access in these mountainous areas, there is a lack of deep and subsurface data (heat flow, borehole and seismic profiles, etc). Thus the challenge when studying hydrothermal systems in such contexts is to use all the shallow available data obtained from field studies (i.e., spring temperatures and locations, topography, structural measurements) as well as geochemical analyses of surface waters so as to understand the deep processes involved (e.g., Belgrano, 2015). In addition, numerical modelling of hydrothermal systems has often been applied during the last 30 years to explain hot spring occurrences, and to explore their controlling factors (Forster and Smith, 1989; Lopez and

Smith, 1995; McKenna and Blackwell, 2004; Bense et al., 2008; Guillou-Frottier et al., 2013; Magri et al., 2016; Volpi et al., 2017).

Among these factors, the topography primarily controls advective heat transfer in the crust (Forster and Smith, 1989; López and Smith, 1995, Gleeson and Manning, 2008). Firstly, isotherms in the shallow crust follow the topography above, compressed below valleys and expanded below higher relief (Braun, 2002; Glotzbach et al., 2009). However, isotherms can be disturbed by other factors such as tectonic movements, erosion and drainage divides, or lateral contrasts in lithology leading to heat refraction effects (Jaupart, 1983; Stüwe et al., 1994; Ehlers and Chapman, 1999; Stüwe and Hintermüller, 2000; Braun, 2002; Glotzbach et al., 2009). Secondly, the topography (actually, the water level elevation and its location with respect to the headwater stream, Gleeson and Manning, 2008) is the main factor responsible for meteoric fluid transfer through mountainous areas, controlling the direction of the fluid pathways and flow rates from the peaks to the valleys (Hubbert, 1940; Forster and Smith, 1988; Ge et al., 2008). The higher the topographic gradient, the deeper the fluids descend, allowing the formation of ”local” or “regional” circulations. In mountainous regions, the flow lines are likely to encounter the warmest zones beneath high reliefs than below flat areas. In such contexts, it is not clear if the topography is sufficient to drive fluids to deep enough levels to attain high temperatures, and how does the topography control hydrothermal fluid circulation and the distribution of springs.

The impact of permeability on hydrothermal systems has also been systematically identified as a critical factor in numerical models (e.g. Forster and Smith, 1988, 1989; López and Smith, 1995; McKenna and Blackwell, 2004). The presence of faults is not necessary to produce hot springs (e.g. Cox et al., 2005; Thiebaud, 2008), however, faults are permeability

heterogeneities in the crust which are known to affect hydrothermal fluid transfer and hot spring location (Faulds et al., 2010), especially at their intersections (Curewitz and Karson, 1997; Person et al., 2012; Belgrano et al., 2016). These studies are mostly related to extensional environments that involve highly permeable active faults and associated sedimentary basins, which favor free convection. Moreover, the high concentrations of hot springs in tectonically active areas can also be explained by fracture opening and breccia formation during coseismic events, which temporarily enhance fault permeability (Faulds et al., 2010; Howald et al., 2015). However, faults in orogenic contexts are often dormant, highly active faults being located towards the front of the range, at the base of the prism, and sometimes inner between major units. In addition, the cores of ranges frequently involve basement rocks uplifted during the combined effect of duplex formation and erosion (e.g., Malavieille and Konstantinovskaya, 2010). Unfortunately, the permeability values of the crystalline rocks constituting the basement are more often estimated than properly measured, the large ranges of values differing according to the scale of measurement (Brace, 1984; Clauser, 1992). In the field, the permeability values are usually low and related to the fracturing state (Brace, 1984). In addition, the evolution of permeabilities with depth is often considered as diminishing because of the effect of confinement on fracture opening (Ingebritsen and Manning, 1999; Saar and Manga, 2004; Earnest and Boutt, 2014). Such depth-dependent permeability is often used in numerical models to explain the spatial distribution of subsurface thermal anomalies (e.g. Garibaldi et al., 2010; Guillou-Frottier et al., 2013). However, this assumption is actually not sufficiently constrained by deep data, and other factors (tectonics, lithology) seem to control the evolution of permeability with depth (Ranjram et al., 2015; Taillefer, 2017). In orogenic belt contexts involving low basement permeability and dormant faults, it is unclear how hydrothermal fluid circulation might occur.

For these reasons, the hierarchisation of the factors controlling hydrothermal systems in orogenic belt environments, especially hot spring locations, merits more investigation. Because the topography of mountainous regions is controlled by faults offsets, but also by erosional processes, this hierarchisation is usually complex in three dimensions. López and Smith (1995) show, in a theoretical 3-D numerical model, that the topography along faults also influences the hydrothermal flows, and numerical simulations have never to our knowledge explored this. Most of the recent numerical studies on hydrothermal systems now involve 3-D topography, sometimes simplified as being flat or slightly sloping (Sonney and Vuataz, 2009) or cylindrical (Magri et al., 2016), but also using realistic topography derived from DEMs (Digital Elevation Models) (Craw et al., 2005; Sutherland et al., 2017; Volpi et al., 2017). However 3-D model geometry built from a complex topography and fault traces, and constrained by fieldwork, is just beginning to be implemented in numerical models (Sutherland et al., 2017).

The Têt hydrothermal system (Figure 1), that is located in the eastern part of the Pyrenean range (France), lies at the interface between extensional and orogenic belt contexts. Twenty-nine hot springs grouped into four main clusters with temperatures ranging from 29 to 73°C are aligned along the 80-km-long dormant normal Têt fault (Krimissa, 1995). The regional tectonic is largely polyphase and has inherited deformations from the Hercynian and Pyrenean orogeneses, and from Neogene extension associated with the opening of the Golf of Lion (Guitard et al., 1998). The current seismicity is low (< 4 Mw), poorly localized (Souriau and Pauchet, 1998), and the stress field is weakly constrained (Taillefer, 2017). High reliefs (2910 m for the highest altitude) formed from the accumulation of the Pyrénées uplift during Eocene time and from the Têt fault's main offset during the Oligo-Miocene period (≈ 2000 m, Maurel, 2003), are incised by alluvial and glacial valleys (Delmas et al., 2009; Calvet et

al., 2014). 2-D analysis of the topographic gradient and serial profiles performed by Taillefer et al. (2017) shows that the highest reliefs (the highest topographic gradient and the mean altitude integrated over their full width) are related to the strongest hydrothermal activity, i.e., the highest number of resurgences and the highest temperatures. The Têt fault juxtaposes basement rocks (gneiss and granite) with metasediments and localized syntectonic basins that show no spatial correlation with hot springs (Taillefer et al., 2017). Hot springs are mainly located in the Têt fault footwall, in the highly fractured crystalline rocks of the damage zone in close proximity to the cataclastic core zone (Taillefer et al. 2017). This example raises the question of how a hydrothermal system in an orogenic belt associated with faults is organized, and which processes primarily control it.

To address these various questions, this study proposes a new and inexpensive method for geothermal exploration at a large scale, in mountainous regions with sharp topography, where geophysical methods have not been operated. New hydrochemical data from the Têt hydrothermal fluids allow determining their altitudes of infiltration and their temperatures at depth. In a second section, a first 3-D numerical model of the Têt hydrothermal system is presented and explored with a parametric study of the role of fault and basement permeability. We focused on a sensitivity analysis on this parameter, allowing gain insights into the driving processes for this hydrothermal system. In other words, the general approach consists in comparing results of numerical models with spring features (temperatures, locations, and temperature at depth and infiltration altitudes given by geochemical data) to constrain the processes and unknown values of permeability. It accounts for a detailed topography based on a DEM and a fault network derived from a 3-D geological model constrained by previously acquired structural field data (Taillefer et al., 2017, Taillefer,

2017). The results enable insights into the impacts of 1) 3-D topography on fluid flow patterns, and of 2) basement and fault network permeabilities on spring temperatures.

2 Geological and hydrological setting

2.1 Geological setting

The Pyrénées result from the N-S collision between the Iberic and European plates during the Eocene (60-40 Ma, Choukroune et al., 1973; Roure et al., 1989). Duplexing and subsequent erosion have exposed basement rocks at the surface in a central part of the belt called the "Axial Zone". The study area (Figure 1) is virtually unaffected by any deformation arising from the Pyrenean orogenesis, except for a diffuse N-S fracturing (Taillefer, 2017).

The lithologies that compose the basement in the study area are the Proterozoic to Cambrian metasediments of Canaveilles and Jujols, alternating with Ordovician gneisses of the Canigou-Carança dome, all intruded by the late-Hercynian Mont-Louis granites (Autran et al., 1986; Guitard et al., 1992, 1998). Some mylonitic Hercynian faults, e.g., the Nord-Canigou Mylonitic Overthrust (*Chevauchement Mylonitique Nord-Canigou*, CMNC, see Figure 1) are crosscut by brittle normal faults resulting from the Oligo-Miocene extension. During this period, a general extension in Western Europe led to the opening of the Gulf of Lion (Seranne, 1999).

In the eastern Pyrénées, the E-W structures of the Pyrenean range are crosscut by the NE-SW Têt fault. During the main period of activity, between 34 Ma to 5 Ma, with the deformation peak during early Oligocene (Maurel, 2008), this 80-km-long normal fault accumulated more than 2000 m of offset (Mauffret et al., 2001; Maurel, 2003; Delcaillau et al., 2004; Maurel et al., 2008). This produced a specific morphology (Figure 1) including: 1) -

an elevated topography in the Têt fault footwall, divided into three moutain massifs with maximum highs around 2900 m, i.e., Puigmal, Carança and Canigou, corresponding to the three segments of the fault (see Taillefer et al., 2017); and 2) the Cerdagne and Conflent flat-lying sedimentary basins in the hanging wall, separated by the Planès topographic high (1600 m). This constitutes the watershed between the Segre and Têt rivers, which flow to the west and east, respectively. The hanging-wall topography is moderate, with the 2000-m-high Serre de Clavera range separated from the Carança range by the Têt valley.

Other NE-SW brittle faults, e.g., the Py fault that connects to the Têt fault, see Figure 1, exist in the area, however there is no information concerning their offsets, which are necessary smaller than that of the Têt fault (Taillefer, 2017). These faults, including the Têt fault, seem to have been reactivated during the upper Miocene to the lower Pliocene, but the offsets would be small (between 150 and 300 m, Carozza and Baize, 2004; Delcaillau et al., 2004) to nonexistent (Maurel et al., 2008). The recent activity of the Têt fault is still being debated (Briais et al., 1990; Philip et al., 1992; Calvet, 1999; Delcaillau et al., 2004; Calvet et al., 2014). Some authors mention evidence of dextral displacements on the Têt fault from the mid-Miocene to Quaternary (Cabrera et al., 1988), but also sinistral transtensional displacements only during the Quaternary (Carozza and Delcaillau, 2000; Delcaillau et al., 2004). Although triangular facets along the Têt and the Py faults are interpreted by Brais et al (1990) and Calvet (1999) as the manifestation of major Quaternary activity, these structures are now reinterpreted as differential erosion (Petit and Mouthereau, 2012). However, evidence of normal and even reverse metric-scale displacements within Quaternary terraces (Philip et al., 1992; Calvet, 1999; Goula et al., 1999; Calvet et al., 2014), raise questions about the recent kinematics of the Têt fault. Despite an alignment of hypocenters in the vicinity of the Têt fault (Souriau and Pauchet, 1998), the seismic activity is moderate

(magnitude 2 to 4) and focal mechanisms do not enable a precise definition of the tectonic regime (Souriau and Pauchet, 1998; Goula et al., 1999; Lacan, 2012). Moreover a synthesis of stress field data by Taillefer (2017) does not permit us to identify the recent or current tectonic regime nor its origin. The seismicity in the area is interpreted to be related to readjustment/exhumation of the Pyrenean range caused by its current erosion (Carroza and Baize, 2004; Vernant et al., 2013; Genti, 2015).

Finally, numerous NW-SE faults, potentially inherited from the Hercynian range (Autran et al., 1986; Guitard et al., 1992, 1998; Barbey et al., 2001; Padel, 2016), show brittle deformation (Taillefer, 2017). Their localisation and abutting relationships with respect to the NE-SW Neogene faults suggest that they could be syn- or even post-Pliocene (Taillefer, 2017), such as faults with similar strikes in Catalonia, 50 km south of the Têt fault (Saula et al., 1994; Tassone et al., 1994; Lewis et al., 2000).

2.2 Hydrogeological setting of the thermal springs

Twenty-nine hot springs align along the Têt fault, principally in its footwall (Figure 1, Taillefer et al., 2017). The field and geomorphological study by Taillefer et al. (2017) highlights that the hot spring locations and the intensity of the hydrothermal activity (number of springs and their temperatures) are principally linked to the topography. More precisely, simple 1-D topographic profiles perpendicular to the Têt fault suggest that springs are located at the base of the highest topographic gradients. Such 2-D results were however obtained without accounting for all the surrounding topography, whose 3-D features necessarily influence fluid circulation. Taillefer et al. (2017) also ranked the factors that seem to favor hot spring occurrence: 1) the lithology (crystalline rocks close to a contact, faulted or not, with metasediments); 2) the Têt fault's intersections with brittle NW-SE faults (and therefore

their damage zones) that are suspected of recent activity (Taillefer, 2017); and 3) the presence of mylonites.

The twenty-nine hot springs are divided into four principal sites that may contain either one spring or several clusters (Figure 1, Taillefer et al., 2017), from the West to the East:

- Llo has one spring at 29.1°C emerging in the fractured gneiss of the Têt fault damage zone,

- The Saint-Thomas-les-bains/Prats-Balaguer site is divided into two close clusters, containing a total of eight springs with temperatures between 30.7°C and 60°C. They emerge in crystalline rocks close to a contact with metasediments. Numerous faults crosscut in the vicinity, including the WNW-ESE Prats fault.

- The Thues-les-bains/Canaveilles site contains two clusters, the first one located in the Têt fault footwall and the second in its hanging-wall. The Thues-les-bains cluster has ten springs with temperatures between 35 and 73.2°C (the hottest spring in the area), emerging in the CMNC mylonites. The three springs at Canaveilles, whose temperatures range between 52.2 and 60.1°C, emerge in gneiss close to a normal contact with metasediments.

- Vernet-les-bains counts seven springs with temperatures between 36.1 and 55.8°C, located 1 km to the south of the Têt fault. They emerge in the CMNC mylonites that juxtapose gneiss in its footwall with metasediments.

Previously, only the study by Krimissa (1995) and reports from the BRGM (French Geological Survey, Courtois et al., 2004; Ladouche et al., 2014; Petit et al., 2014) have provided geochemical data from the area. The water is alkaline, with a high pH ≈ 9, and the concentrations of Ca and Mg ions are low. The waters' stable isotopes indicate that the hydrothermal fluid has a meteoric origin, and that infiltration areas are located above 2000 m of altitude (Krimissa, 1995, see dashed white lines in Figure 1). No variations of temperature with time have been observed (Petit et al., 2014). The $^{87}Sr/^{86}Sr$ and $^{36}Cl/Cl_{total}$ ratios, and the weak mineralization of the fluid would indicate that it circulates only through crystalline rocks with similar chemical signatures. Mean residence times, calculated from ^{14}C, range between 5,000 and 13,000 years. Finally, geothermometry indicates equilibrium temperature around 100°C (Krimissa, 1995). However, that study does not provide the precise location of the sampled hot springs, and the Llo and Prats-Balaguer sites were not sampled. Moreover, in the last decade, new methods for studying hydrothermal systems, involving the lithium isotopic ratio, have been developed (Millot and Négrel, 2007; Millot et al., 2007). For these reasons, we present below new geochemical analyses carried out on ten hot springs in the study area.

3 Geochemical constraints

3.1 Methods

At least one hot spring per cluster is sampled (see supplementary materials for the locations and features of the sampled hot springs). The hottest spring in the cluster is always sampled because it is assumed to be less mixed with surface water. Colder springs are sometimes sampled within a single cluster, in order to highlight potential fluid mixing.

The general physico-chemical features of the thermal waters are systematically measured. Measuring the ionic concentrations enables a determination of the fluid's origin and analysis of the similarities of the fluid signatures from different springs. Using a MC-ICPMS, physico-chemical interactions between the fluids and the rocks are also explored by measuring, the lithium isotopic ratio that reveals a relationship with temperature (Millot et al., 2007).

Infiltration altitudes are calculated from the waters' stable isotopes $\delta^{18}O$ and $\delta^{2}H$, using a local $\delta^{18}O$ gradient of 0.24‰ per100 m, established by Krimissa (1995):

$$\delta^2 H = 7.7 \times \delta^{18} O + 9.9 \quad (1)$$

The principal drawback of this method is the lack of knowledge of the past-climate, which may affect isotopic fractionation. In the Pyrénées, the last glaciation ended no more than 11,000 years ago (Delmas, 2009). Because infiltration of the Têt hydrothermal fluids is relatively recent (5,000 to 13,000 years, Krimissa, 1995), the climate during this period may reasonably be considered to be similar to the current one, thus introducing no bias in the altitude estimation. Moreover comparisons of the isotopic data with world (DMEM) and local (DLEM, from Négrel et al., 2007) meteoric water lines enable the fluid's origin to be determined.

The ionic concentrations of the thermal fluid are also used to calculate various geothermometers that indicate the temperatures of equilibration between the fluid and the surrounding rocks at depth, i.e., the maximum temperature reached by the thermal fluid (White, 1965). Those applied in this study are the silica (quartz without steam lost, quartz

with steam lost, chalcedony, Fournier (1977), the Na/Li (Fouillac and Michard, 1981), and finally the Na/K (White, 1965; Ellis, 1970).

3.2 Results

3.2.1 Fluid-rock interactions

The physico-chemical features, and the ionic concentrations of the thermal fluid (see supplementary material) are similar for all the springs (Figure 2). The only exception is the Saint-Louis spring (Thues-les-bains cluster), which exhibits anomalies of pH, dissolved O_2, and also the following ions: Ca^{2+}, $NH4^{+}$, $CO3^{2-}$, HCO^{3-}, and NO^{3}, suggesting a mixing with surface water.

Differences of temperatures for the other sampled springs in a single cluster cannot be explained by mixing with cold water. The hydrothermal fluids are generally highly concentrated in Na ion, and poorly concentrated in Cl ion, compared to the sea and to the rain water lines (Figure 2a), thus confirming their meteoric origin. The ionic concentrations are similar for all the Têt hot springs when compared with Dorres-Colomer (another hydrothermal system in the north of the Cerdagne basin, see Figure 1), and similar for the various springs in a single cluster. The Gr. Amont Rivière spring (Canaveilles cluster) shows a lower Cl concentration and a higher Na concentration than the other springs. The low Na concentration of the Saint-Louis spring (Thues-les-bains cluster), closer to the rain water line, supports the mixing hypothesis.

The Na/Li ratio is similar for all the Têt springs (Figure 2b), and smaller than those from Dorres-Colomer. The lithium isotopic ratio $\delta^{7}Li$ is slightly smaller for the Vernet-les-bains and Llo springs than for the other Têt springs, but still high compared to that ratio in the

Dorres-Colomer springs. The latter is close to the lithium isotopic ratio of a crystalline basement (Millot et al., 2010), which is consistent with the rocks with which the fluids are supposed to react (Ladouche et al., 2014). The lithium isotope ratios of the Têt springs correspond to the signatures of carbonates (Hoefs and Sywall, 1997). This particular signature will be discussed later, in section 5.3.

3.2.2 Infiltration altitude

The position of the Têt fluids in the water-stable isotope space ($\delta^{18}O$ / $\delta^{2}H$, Figure 2c), surrounded by the world and local meteoric-water lines, confirms their meteoric origin. Three groups are identified:

1. Thues-les-bains (Saint-Louis excepted), Saint-Thomas-les-bains/PratsBalaguer, and Gr. Amont-Rivière (Canaveilles cluster),

2. Vernet-les-bains,

3. Llo (intermediate between these two poles).

The average infiltration altitude for the fluid is around 2100 m for all the springs, and potentially lower at Vernet-les-bains and Llo than for the other springs (see the individual altitude of infiltration for each spring in supplementary materials).

3.2.3 Fluid temperature at depth

The profiles of temperature at depth along the Têt fault (Figure 2d) calculated from the silica geothermometers mimics the profile of spring temperatures at the surface along the Têt fault. Temperatures are highest at the center of the profile (Thues-les-bains/Canaveilles,

100 to 135°C) and decrease on both sides of it. Temperatures fall between 80 and 110°C at Llo, between 95 and 120°C at Saint-Thomas-les-bains/PratsBalaguer, and between 90 and 120°C at Vernet-les-bains. The Na/K profile is close to the silica profiles, except for the lower temperature (100°C) at Saint-Thomas-les-bains/Prats-Balaguer. The Na/Li profile is flatter, with temperatures at depth around 100°C for all the springs except Vernet-les-bains (90°C).

Given that meteoric fluids infiltrate at high altitudes (at a temperature of ≈ 5-10°C) and emerge at ≈ 30-80°C, fluid pathways from the highlands to the springs must extend down to several kilometres below sea level, where ambient temperatures range between 80 and 130°C. To test this hypothesis, it is necessary to simulate fluid flow through the shallow crust from the mountain range to the permeable fault. In the following numerical modeling approach, fluid flow can be driven by topography and/or by buoyancy. Because permeability is the most variable and unknown petrophysical property, we focus our sensitivity study on this parameter. The main objective of the numerical models detailed below is to reproduce (simulate) the emergence of hot springs (location and temperature values) by varying the most uncertain parameter, i.e., the permeability of the fault zone. Similarly, the permeability of the host rocks, although qualitatively constrained by structural observations (Taillefer, 2017), also represents an additional variable. The other physical properties (rock mass density, porosity, thermal capacity, thermal conductivity, thermal expansion coefficient) do not vary greatly and do not significantly affect the hydrothermal regime in comparison to permeability.

4 Spatial distribution of thermal anomalies related to 3-D topography: numerical modeling

This section explores the hydrothermal processes occurring in a coupled heat and fluid flow model that employs a geometry constructed from 1) a realistic topography based on a DEM, and 2) a 3-D structural model constrained by structural field data acquired at the surface. The downward extension of surface data (fault dip, intensity of fracturing) may be questioned and will be discussed later. To implement this geometric and geological model within the COMSOL Multiphysics™ software, the Darcy law and the heat transfer equation have been coupled in the 3-D model, through a similar numerical procedure to that used by Guillou-Frottier et al. (2013). The results of the 2-D numerical models of McKenna and Blackwell (2004) have been used as calibration models, and reproduced in COMSOL Multiphysics™ by Taillefer et al. (2017).

4.2 Numerical method: from 3-D geological model to 3-D physical processes

4.2.1 Governing equations and temperature-dependent parameters

Faults and basement are considered to be porous and permeable media where conservation laws can be applied. The heat equation for a homogeneous and isotropic medium, as regards convective heat transfer, is:

$$\rho_s Cp_s \frac{\partial T}{\partial t} = \lambda_s \Delta T + A - \rho_f Cp_f \vec{\nabla} T . \vec{u} \qquad (2)$$

where T (°C) is the temperature, ρ_s (kg.m^{-3}) the medium's density, Cp_s (J.kg^{-1}K^{-1}) its specific heat capacity, λ_s its thermal conductivity (W.m^{-1}.K^{-1}), A (W.m^{-3}) the heat production,

ρ_f (kg.m^{-3}) the fluid density and Cp_f (J.kg^{-1}.K^{-1}) the fluid specific heat and u (m.s^{-1}) the fluid velocity.

For porous and permeable media the Darcy law describes fluid motion driven by a pressure gradient such as:

$$\vec{u} = -\frac{k}{\mu}(\vec{\nabla}p - \rho_f \vec{g}) \quad (3)$$

where k (m^2) is the medium's permeability, μ (Pa.s) the fluid viscosity, p the pressure (Pa) and g (m.s^{-2}) the acceleration of gravity. The fluid is assumed to be incompressible and mass conservation requires:

$$\nabla.\vec{u} = 0 \quad (4)$$

The coupling between the heat transfer equation and Darcy's law is obtained through the fluid velocity field in equations (2) and (3). Further, temperature (the other coupling variable) appears in both equations, since fluid density and fluid viscosity are temperature-dependent, as in:

$$\mu(T) = 2.414\ 10^{-5}\ .exp\left(\frac{570}{T+133}\right) \quad (5)$$

as defined in Rabinowicz et al. (1998), where μ (Pa.s) is the fluid dynamic viscosity and T (°C) the temperature, and :

$$\rho_f(T) = 1002.4 - 0.1905.T - 0.0025\ .T^2 \quad (6)$$

where ρ_f (kg.m^{-3}) is the fluid density.

4.2.2 Constraining data, geometry and mesh

4.2.2.1 Data and hypotheses

The structural field data used to build the 3-D geological model are presented in Taillefer et al. (2017) and Taillefer (2017). Faults have been traced using remote sensing and verified or detailed with numerous control points in the field. The fault features (dip direction, dip, organisation and constitution of the fault zones) have been analysed at the fault zone outcrops. A three months field campaign allowed collecting geological data (lithology, structural features, deformations, and at least 30 fracture measurements per outcrop) of more than 300 outcrops distributed near the faults and the hot springs but also far away in the mountain range (i.e. the infiltration areas, see sections 2.2 and 3.2.2). The results are the geological maps and cross-sections in Taillefer et al., 2017 simplified in Figure 1 as a structural scheme, the cross-sections being presented in Supporting Information, and outcrops interpretation giving the size of the damage zone (Taillefer et al., 2017). Additionally, lineaments maps and fracture features measured in the field allow respectively discussing the fracture distribution and effects according to the lithology, and consequently the permeability (Taillefer, 2017).

As detailed in section 2.1, the basement of the study area is mainly composed of crystalline rocks (see cross-sections in Supplementary Material), excepted in the western and eastern parts of the study area, where the Têt fault (respectively the CMNC) juxtaposes gneiss and metasediments. As a first approximation, these two lithologies are treated as a homogenous unit in the model. This choice is discussed in section 5.2. The two basins of

Cerdagne and Conflent (see Figure 1) have small extensions and depths and do not localize any hot springs (Taillefer et al., 2017), and are thus not considered.

In order to study only the main processes acting in the system, and not adding unnecessary uncertainties, the used geometry is here simplified by considering only the three principal faults among those previously mapped (Figure 1): the Têt, the Py, and the Prat faults (Figure 3a).

The Têt fault trace is well constrained at the surface at Llo, Thues-entre-Valls and Thues-les-bains and dips between 50 and 70° northwards. With respect to Figure 1, it is simplified in the model as a unique segment. New seismic profiles crossing the Têt fault in eastern Pyrénées (Diaz et al., 2018) fail to precisely image the Têt fault at depth..However, a potential displacement of the seismic reflector between 5 and 10 km could confirm its continuity at such depth (see their Figure 5). The Têt fault core is an alternation of fractured gneiss and cataclasite lenses. The size of the footwall damage zone (the hanging wall is hardly visible) is difficult to evaluate because vegetation quickly mask the outcrops, but is estimated around 100 and 200 m.

The Py fault, the second most important fault in the area, separates the Canigou from the Caranca massifs, connecting to the Têt fault east of Vernet-les-bains, and west of Llo. The fault zone is 300 m large and essentially cataclastic. This fault dips between 60 and 80° to the north, its NE-SW strike deviates near its centre, where it is crosscut by a NW-SE fault (the "Coum de Bassibes" fault, see Figure 1). Because of the absence of outcrop, the westward continuity of the Py fault may be discussed (Guitard et al., 1998). Its geometry is here simplified as a continuous and unique fault.

Finally, the WNW-ESE Prats fault is a cataclastic subvertical fault that connects to the Têt fault close to Saint-Thomas-les-bains (500 m) and across the Prats-Balaguer hot springs (Figure 1).

4.2.2.2 Building the geometry and mesh

We then use the GeoModeller^{TM} software that combines topographic data (DEM) with surface structural data (faults, stratigraphic contacts) to create a 3-D geological model consistent with the structural geology principles (constant strata thickness, overlaps, cross-cutting relationships; e.g., Calcagno et al., 2008). The GeoModeller^{TM} uses field structural measurements (dip and dip-direction) in various control points, together with the fault traces obtained from surface mapping (Figure 1) to extrapolate them at depth, and then to build the 3-D geological model of the study area (Figure 3a). Faults are modelled as surfaces in a volume that represents the basement.

A thickness of 300 m is assigned to the faults, corresponding to an average size of fault zone, i.e. the volume where the permeability will be tested independently of the basement.

The upper surface of the model corresponds to the realistic topography of a 30 m DEM resolution from the USGS (Figure 3b). The highest elevation of the geometry is the highest peak in the area (the Puigmal: 2913 m). The base of the model is fixed at a depth of 5,000 m. The area covered by the model is 43 km long (E-W) and 32 km wide (N-S), and includes all the hot springs. Without any information about the level of the water table below the mountain range, its location is approximated as being the topographic surface. This approximation is often valid for crystalline rocks aquifers in high mountain ranges (Tiedeman

et al., 1998; Bossong et al., 2003; Caine et al., 2006) where the water table location, close below the surface, poorly influences the regional flows (Gleeson and Manning, 2008).

To avoid errors and overlong computational time, a mesh convergence study was performed by refining the mesh successively until a similar solution to the previous one (within a difference of about 1°C) was found. It turned out that stable solutions were obtained for about 500,000 elements. A polygonal mesh grid of 503,976 elements has accordingly been built over the entire geometry (Figure 3b). The mesh is refined around the topographic complexities, the fault planes and fault intersections. The mean and smallest element sizes are respectively 827 m and 6 m in the main volume, and 609 m and 8 m around the faults.

4.2.3 Model parameters and simulations

The fault and basement permeabilities excepted, fluid and rock properties are common to all simulations (Table 1). Three kinds of simulation were computed, using different geometry settings (Table 2):

- Simulation 1: Homogeneous basement without any faults,

- Simulation 2: Homogeneous basement involving the Têt fault only,

- Simulation 3: Homogeneous basement involving the Têt, Py and Prats faults.

Among all the petrophysical properties that have to be implemented in the model, permeability is by far the most poorly-known property, with a range of possible values spanning several orders of magnitude. In this study, the selected permeability values are consistent with the range of crystalline rock permeability values encountered in the literature (Brace, 1984; Sonney et Vuataz, 2009; Moeck, 2014; see Section 1 for a discussion of the

current state of knowledge concerning the permeability of crystalline rocks, and Table 2 for the permeability combinations used in the simulations). Although lateral lithological variations have been observed in the field (see Section 2.1), the permeability of the lithologies encountered in the study area (metasediments, granite, gneiss) is mainly linked to the fracture network. Thus, the basement is here considered to be a single homogeneous unit and is tested for two permeability values: $k_b = 10^{-17}$ m^2 (impermeable) and $k_b = 10^{-16}$ m^2 (fairly permeable, that is consistent with the fracture density and opening study by Taillefer, 2017). The Têt fault damage zone is thought to have enhanced the basement permeability (Taillefer et al., 2017). However, because the recent fault activity (see Section 2.1) and fracture sealing in the damage zone are poorly constrained, a large range of permeability was tested (Table 2) consistently with values encountered in the literature for faults in equivalent basement rocks (Evans et al., 1997; Sonney et Vuataz, 2009). The Py and Prats faults being of smaller importance than the Têt fault (Taillefer, 2017), an intermediate permeability of $k_{fPy} = k_{fPr} = 5.10^{-15}$ m^2 is assigned in the last simulation.

4.2.4 Boundary and initial conditions

4.2.4.1 Flow conditions

An altitude-dependent atmospheric pressure $P_{atm}(z)$, from the International Civil Aviation Organization Standard Atmosphere, is imposed at the topographic surface (Figure 3c):

$$P_{atm}(z) = P_0 \times \left(1 - \frac{0.006z}{288.15}\right)^{5.255} \quad (7)$$

where P_0 = 10^5 Pa is the atmospheric pressure at sea level and were z (m) is the altitude. Below the surface topography, a hydrostatic pressure gradient $\rho.g$ is added to P_0. No flow is allowed through the lateral limits of the model.

4.2.2.2 Thermal conditions

Because of the lack of regional deep-level data, a constant heat flow q_0 = 0.09 W/m^2, consistent with the heat flow map of France by Lucazeau and Vasseur (1989), is imposed at the base of the model. The lateral limits of the model are thermally insulated.

In order to allow for temperature variations at the surface (cold areas at high altitudes but also warm zones where hot springs emerge), a mixed thermal boundary condition like that used in Magri et al. (2016) is applied to the topographic surface:

$$Q = h(T_0 - T) \quad (8)$$

where Q (W.m^{-2}) is the surface heat flow, h (W. m^{-2}.K^{-1}) a coefficient of heat transfer and T_0 (°C) the reference temperature at the surface (chosen to be 10°C).

In order to impose a realistic thermal boundary condition, a sensitivity analysis of the heat transfer coefficient h was performed. The condition applied to the topographic surface needs to satisfy: 1) a realistic temperature at the surface (5-10°C in the study area), and 2) potential convective flows allowing hot fluid emergence. The h value has therefore been calibrated so as to combine realistic temperatures for (i) the fluid infiltrated at the model surface, and (ii) the hot fluids that rise up to the model surface (calibration details are available in the Supplementary Materials).

To obtain consistent temperatures at the surface (between 5 and 10°C) while emergence temperatures may reach 70°C, the optimum *h* value appears to range between 0.017 and 0.025 $W.m^{-2}.K^{-1}$. Lower values cause all the basins and valleys to reach 30°C, a value which is not observed in the field. Higher values do not permit thermal convection to affect the surface temperature. Accordingly, *h* is assigned the value of 0.02 $W.m^{-2}.K^{-1}$, which is a good intermediate figure allowing convection to produce positive thermal anomalies at the surface (up to 70°C) without inducing unrealistic temperatures in the valleys and basins. Using this value, the few areas at high altitude (above 2000 m) exhibit low temperatures (5-7°C) while all other areas show surface temperature of 10 +/- 2 °C.

The initial conditions for the model are a hydrostatic pressure and a purely conductive thermal state, from which a steady-state is computed. Transient evolution of permeability, topography, or pressure, will be discussed in section 5.

4.3 Results

4.3.1 Preliminary study of the thermal regime: the critical Rayleigh number

The Rayleigh number (Ra) enables determination of the thermal regime within the model, and in particular the critical permeability value from which free convection is likely to start (Magri et al., 2016). For an infinitely long homogeneous porous medium (Lapwood, 1948), Ra is defined as:

$$Ra = \frac{K\ L\ \alpha\ \Delta T}{D_\lambda} \quad (9)$$

where *K* ($m.s^{-1}$) is the hydraulic conductivity, related to the permeability *k* (m^2) by:

$$k = K\left(\frac{\mu}{\rho_f g}\right) \quad (10)$$

L (m) is the thickness of the medium in which the flow takes place, α (K^{-1}) the coefficient of thermal expansion and ΔT (°C) the difference in temperature between the upper and lower limits of the medium. The tensor of thermodispersion D_λ is defined by:

$$D_\lambda = \frac{\phi\,\lambda_f + (1-\phi)\lambda_s}{\rho_f\, Cp_f} \quad (11)$$

where ϕ is the porosity, ρ_f ($kg.m^{-3}$) the fluid density, Cp_f ($J.kg^{-1}.K^{-1}$) the thermal capacity of the fluid, and λ_f and λ_s the fluid and solid thermal conductivity, respectively. The value of ρ_f is taken at the minimum temperature (here 10°C). Given (i) a basement thickness between the infiltration area's altitude (+2000 m) and the model's base (-5000 m) of 7000 m, (ii) a basement permeability k_b of 10^{-16} m^2, (iii) a temperature difference of 270°C between the top and the base of the model, and (iv) fluid and rocks properties as indicated in Table 1, the computed Rayleigh number is Ra ~ 0.34.

This value is much smaller than $4\pi^2$, the critical Rayleigh number Ra_c from which free convection is likely to start for an infinitely long homogeneous porous medium. This means that the thermal regime in the basement is probably not driven by buoyancy flow but by topography (forced convection only). However, for a finite medium including faults, the critical Rayleigh number depends on the faults' dimensions, and can be expressed by the ratio between the fault width and height.

Analytical and numerical simulations by Malkovsky and Magri (2016) show that, given the geothermal gradient in the study area, the critical fault permeability kf_c at which

convection is likely to start within the fault is calculated by assuming $Rc_f/4$ (e.g., Figure 4 in Malkovsky and Magri, 2016). For a fault width d =300 m, and a fault altitude in the model surface around 1000 m (which corresponds to a fault height of H = 6000 m), $Rc_f/4 = 68$. The inferred critical permeability for which thermal convection may occur in the fault is thus (using this value of 68 and Equations 9 and 10):

$$kf_c = \frac{68\times[(0.1\times0.6+0.9*2.5)/(1000\times4180)]}{10^7\times6000\times10^{-4}\times270} \sim 2\ 10^{-14}\ \mathrm{m}^2 \qquad (12)$$

Consequently, in the model computed here, the free convection within the fault is likely to start at a fault permeability higher than 2.10^{-14} m^2.

4.3.2 Single-fault model

4.3.2.1 Thermal anomalies at the surface

Small, cold thermal anomalies appear at the surface along the Têt valley when the permeability is similar in the basement and in the Têt fault (10^{-16} m^2 everywhere, Figure 4a). In this case, only two narrow thermal anomalies (around 25°C) are aligned along the Têt fault, between St-Thomas/PratsBalaguer and Thues, and east of Thues/Canaveilles. No thermal anomaly is visible at Llo or at Vernet.

For a basement permeability $k_b = 10^{-16}$ m^2 and a Têt fault permeability $k_{fT} = 10^{-14}$ m^2 (Figure 4b), four positive thermal anomalies are aligned along the Têt fault, corresponding to the observed clusters. The largest thermal anomaly, located between Saint-Thomas/Prats-Balaguer and Thues/Canaveilles, is also the hottest (70°C at Thues). The other thermal anomalies at Llo, east of Canaveilles, west of Vernet, and at Vernet, are smaller and temperatures reach 50°C. Temperatures of the thermal anomalies at Thues-les-bains and

Saint-Thomas vary as a function of the basement and the Têt fault permeabilities (Figure 4c). For low permeability values within the Têt fault ($k_{fT} < 10^{-15}$ m^2), the temperatures at Thues and Saint-Thomas are around 20°C for basement permeability $k_b = 10^{-17}$ m^2, and 30°C for $k_b = 10^{-16}$ m^2. For good permeability values within the Têt fault ($k_{fT} > 10^{-15}$ m$^{2)}$, the higher the Têt fault permeabilities, the higher the temperatures at Thues. Finally, for a high permeability within the Têt fault ($k_{fT} = 10^{-14}$ m$^{2)}$, the temperature at Thues is the highest for $k_b = 10^{-16}$ m^2, reaching 73°C (the maximum observed hot spring temperature). The trend is different or even reversed for Saint-Thomas: temperatures are stable for a basement permeability of $k_b = 10^{-17}$ m^2, and decrease with increasing Têt fault permeability for $k_b = 10^{-16}$ m^2.

The Têt fault and basement permeabilities induce different patterns of thermal anomalies along the Têt fault (Figure 4d). The same peaks of thermal anomaly, with different amplitudes, are observed for all the cases studied. For the case in which the fault has the same permeability as the basement ($k_b = k_{fT} = 10^{-16}$ m^2), the temperature along the fault at the surface ranges between 15 and 28°C, with the maximum temperature at the fault's center (blue curve in Figure 4d). Making the Têt fault quite permeable ($k_{fT} = 10^{-15}$ - 10^{-14} m^2) results in doubling or tripling the amplitude of the peak temperatures in the case of a basement permeability of 10^{-17} m^2 or 10^{-16} m^2, respectively. Observed hot spring temperatures are reproduced at Llo and Thues-les-bains/Canaveilles, and approximately at Vernet for $k_b = 10^{-16}$ m^2 and $k_{fT} = 10^{-14}$ m^2 (light green curve in Figure 4d). However, the hot spring temperatures at Saint-Thomas-les-bains/Prats-Balaguer are not reproduced. Finally, it is interesting to observe that the temperatures between the positive thermal anomalies are lower for a permeable fault than for a sealed one.

4.3.2.2 Thermal anomalies at depth

The location of thermal anomalies at the surface arises from the distribution of thermal anomalies at depth along the fault plane (Figure 5a). Negative thermal anomalies (infiltration areas), associated with moderate downward Darcy velocities, alternate with positive ones (emergences) associated with high upward Darcy velocities, which mostly correspond to the location of the hot spring sites. The highest Darcy velocities ($1.7x10^{-8}$ $m.s^{-1}$) and temperatures are located at Thues (Figure 4d). A large infiltration area along the Têt fault corresponds to the Planes topographic-high (top right of Figure 5a). Darcy velocity vectors diverge eastward and westward from this area, inducing a negative thermal anomaly affecting Saint-Thomas/Prats-Balaguer.

Thus depending on the location, the along-fault flows have different effects on the temperature in the surrounding basement (Figure 5b, see Supplementary Materials for the cross-sections at Llo and Vernet-les-bains). Around the Têt fault, isotherms are depressed at Saint-Thomas/Prats-Balaguer whereas they are elevated at Thues. The wavelengths of the thermal anomaly are ≈ 500 m near the surface and ≈ 4 km at -4000 m. The amplitude of the thermal anomaly decreases with depth.

Flow lines within the model show the origin and pathway of the fluids in relation to the thermal anomalies on surface (Figure 5c). The features of the flow lines related to each thermal anomaly are summarized in Table 3. A large majority of the flow lines contributing to these thermal anomalies come from the mountain ranges in the Têt fault footwall, descend inside the model until they reach a certain depth (sometimes the bottom of the model, see Table 3) where the fluid is heated to 210°C. The deeper the fluid descends, the higher its

temperature. Fluids are directed towards the Têt valley and caught by the Têt fault, which brings them towards the surface, thus creating thermal anomalies, i.e., the hot springs.

The Planes topographic-high (see Figure 1 and Figure 5 a, c) is a separation line for the fluids that infiltrate into the Têt fault. Along the Têt fault at Saint-Thomas/Prats-Balaguer, the emerging flow lines do not descend deep enough to generate hot fluids. However, some flow lines infiltrated at Planes along the Têt fault, which do descend deep enough to heat the fluids (-2000 m), emerge at Thues/Canaveilles. These waters contribute to the high thermal anomalies observed there.

Finally, the flow lines coming from the Têt fault's hanging-wall are caught at depth by the Têt fault and flow eastward at a deep level, without reaching the surface. The only exceptions are the flow lines coming from the Serre de Clavera, the highlands at the north of the valley above Saint-Thomas/Prats-Balaguer, which descend far enough to make an additional positive contribution to the Thues/Canaveilles thermal anomalies (-1950 m, see Table 3).

4.3.3 Multi-fault model (Têt, Py and Prats)

In a permeable multi-fault model (k_{fT} = k_{fPy} = k_{fPr} =5.10^{-15} m^2, Figure 6), fluid circulations also take place along the fault planes, affecting the isotherm distribution (Figure 6a). High-downward Darcy velocities allow infiltration of cold fluids within the mountain ranges, especially in the first kilometer. The Py fault allows considerable fluid infiltration, thus preventing the formation of positive thermal anomalies at the surface.

High upward Darcy velocities are found along the Prats fault, at its intersection with the Py and Têt faults, and at its center where there is a topographic depression. At the intersection between the Py and the Prats faults and at the topographic depression, the fluid is too cold to create a hot emergence. However, isotherms are elevated at the intersection between the Prats and Têt faults. Compared with the single-fault model ($k_{fPr} = k_b = 10^{-16}$ m^2, Simulation 2, Figure 6b), attributing a high permeability to the Prats fault ($k_{fPr} = 5.10^{-15}$ m^2) induces an upwelling of hot fluids originating from infiltration along the Prats fault, and the creation of a positive thermal anomaly at Saint-Thomas/Prats-Balaguer (Figure 6c). It enables duplication of the hot spring temperatures of Saint-Thomas/Prats-Balaguer, unlike the single-fault model (Figure 4d).

5 Discussion

5.1 Relationship between the topography and the distribution of thermal anomalies along the Têt fault

Numerical results suggest that topography (i.e. an elevated water table) is the key factor controlling the fluid pathways and the hot spring distribution in the Têt hydrothermal system. The location of the positive thermal anomalies at the surface of the numerical model (Figure 7a) confirms the field study of Taillefer et al. (2017), which showed that the most intense hydrothermal activity (highest temperature and hot spring number) is related to the highest topography in the Têt fault's footwall. Moreover, the elevations of the infiltration areas in the models correspond to those calculated from water-stable isotopes. Since the topographic gradient controls the depth of fluid infiltration (Figure 5c), it also controls the maximum temperatures reached by the fluids at depth, as indicated by numerical models (Table 3) and confirmed by geothermometry (Figure 7b).

However, the impact of the topographic gradient along the fault on the fluid pathways, although theoretically demonstrated by López and Smith (1995), had never been highlighted for hydrothermal system, previous models having involved a more symmetrical or "cylindrical" topography (e.g. Mckenna and Blackwell, 2004; Magri et al., 2016) or a complex topography without faults (e.g. Craw et al., 2005; Ge et al., 2008; Volpi et al., 2017). Thus, the Planes topographic-high, separating the Têt valley from the Cerdagne basin, acts as a watershed for groundwater infiltrated along the permeable Têt fault (Figure 7c). The resulting alternation of infiltration and resurgence areas controls the distribution of temperatures at all depths along the Têt fault (Figure 7a and d), including the surface. Moreover, the Py fault is exclusively an infiltration structure despite its similarities with the Têt fault (Figure 6a). Further, fluids that flow at depth toward the east along the fault plane (Figure 5c) will never reach the surface because of the regional topographic gradient between the Cerdagne and de Rousillon basins. This suggests that the fault's ability to localize hot springs is also controlled by the fault plane's location with respect to the surrounding topography. Hence, it is crucial to examine both the topography's complexities in 3-D and the fault system patterns to understand the full hydrothermal system, as recently demonstrated for other examples (e.g., Sutherland et al., 2017; Volpi et al., 2017). The location of the water table could be even more critical. If it actually does not correspond to the topography (our hypothesis, see section 4.2.2.2), this could influence the part of the discharge driven by the topography. However, if the water table was positioned 200 - 300 m below the surface, the difference of hydrostatic pressure would be low compared to that within the 3 km layer through which the fluid circulates. Furthermore, the pressure gradients would not be affected. Considering the residence times of the water, the reservoir size should be huge. Thus, the

overestimated quantity of water is likely low compared to the volume of stored fluids, and would probably not influence the final discharge.

The major portion of the Têt valley's topography was acquired during the combined uplifts of the Eocene Pyrenean orogenesis and the Oligo-Miocene extension (≈ 2000 m, Mauffret et al., 2001; Maurel, 2003; Delcaillau et al., 2004; Maurel et al., 2008). Naturally, the relief would have been modified by erosion over the last 5 Ma. However, the 55 m/Ma maximum erosion rates evaluated in the region (Calvet et al., 2015; Sartegou et al., 2018) represent a maximum incision of 350 m of the Têt valley. Moreover the ice cover during the last glaciations was quite limited in the study area (Delmas et al., 2009; Calvet et al., 2014) and has had little effect on the topography (Jarman et al., 2014). Thus it seems reasonable to assume that the currently observed topography used in numerical models (Section 4.1.2) approximates the early Pliocene one, and that the potential error does not affect the highest topographic gradients involved in the topography-driven transport of hydrothermal fluids. However, the temporal evolution of the permeability with respect to the recent evolution of tectonic stresses (unconstrained and debated in the study area, see Section 2.1) may be more critical, as discussed below.

5.2 Fault and basement permeabilities

2-D numerical models of the Têt hydrothermal system constructed in a previous study (Taillefer et al., 2017) demonstrated the strong impact of the Têt fault's permeability on hydrothermal circulations, as confirmed by the sensitivity study in Section 4.3. The case of a topography-driven hydrothermal system with no permeable fault (or a sealed one, e.g., Simulation 1), is likely to produce weak thermal anomalies (maximum 30°C) at the valley bottom (Figure 4a), i.e., where they are also observed for the highest permeability

simulations. Thus, the topography appears primarily to control hot spring location and temperature, while the permeability acts secondarily to adjust the temperature. The strong thermal anomalies at the surface result from (i) fluid flow in the basement caught by the Têt fault, and (ii) fluid flow infiltrated along the Têt fault. For a fault permeability increase of one order of magnitude, the temperature of positive anomalies may double, while the effect is half as big for the same increment of basement permeability (Figures 4c and 4d).

The alternation of positive and negative thermal anomalies at depth along the faults is described for hydrothermal systems involving free convection (e.g., Magri et al., 2015, 2016). In our more relevant models (Simulation 3), the highest permeability used to the Têt fault is close to the critical permeability $k_{fc} \approx 2.10^{-14}$ m^2 for which free convection is likely to start (see Section 4.2.1). This raises the question of the possibility of developing free convection in the Têt hydrothermal system. However, the all range of permeability values used in the models is not completely realistic. Indeed, permeability probably decreases with depth, both in the basement and in the fault (e.g., Stober and Bucher, 2015, Taillefer, 2017). Consequently, depending on the Rayleigh number, this would decrease the elevation at which convection is likely to occur. The critical permeability would thus have to increase up to an unrealistically high value for this kind of lithology, unless dynamic (time-dependent) permeability is accounted for (Ingebritsen and Gleeson, 2015).

The sensitivity study carried out in this paper may be used to evaluate the effective permeability values that are impossible to measure at this scale. Our results suggest that the Têt fault is still permeable for a fault in crystalline rocks (Bense et al., 2013), although it has been dormant since the Mio-Pliocene (Goula et al., 1999). Moreover the role of the Prats fault, which is required to reproduce the Saint-Thomas thermal activity (Simulation 3, Figure

6), suggests that the NW-SE fault network is also probably permeable. However, fracture networks such as fault damage zones may be quickly sealed by hydrothermal alteration deposits (several thousand to a few million years, Lowell et al., 1993; Renard et al., 2000) without any tectonic activity (Faulds et al., 2010; Howald et al., 2015; Stober and Bucher, 2015). Hence, the recent and current low tectonic activity in the Eastern Pyrénées (see Section 2.1), together with fluid overpressure and favourably oriented stress field, or current seismicity, may suffice to maintain an efficient permeability in the fault entire network. In addition, our study highlights the importance of permeability variations along the Têt fault for the location and temperature of hot springs: i) enhanced permeability at fault intersections as demonstrated by many previous authors (Faulds et al., 2010; Person et al., 2012; Belgrano et al., 2016); ii) the partial sealing of the Têt fault damage zone at Thues-entre-Valls (Taillefer, 2017), which could explain the lack of hot springs at places where numerical models predict a strong positive anomaly (Figure 4d, and see Howald et al., 2015). This suggests that permeability has not been constant throughout the faults (along strike and in depth) over the last 5 Ma. Transient effects on the permeability (sealing by hydrothermal alteration minerals versus tectonic activity such as pressure variations) should be explored in future simulations.

Similarly, our simplified model does not take several considerations into account :

(i) The basement is considered as a homogenous unit of crystalline rocks, without considering permeability variations with lithology. Fluids transfer is here studied at a regional scale, in a range of permeability consistent with the measurements referenced in Clauser (1992) for this scale. Actually, the basement in the area is composed of crystalline rocks and metasediments. In the literature, permeability of these two kinds of rock is sometimes not differentiated because mainly related to fracturing (Freeze and Cherry, 1979; Gleeson et al.,

2011; Ranjram et al., 2015), but simultaneously some data seems to indicate that the permeability range for metasediments is smaller than crystalline rocks (10^{-20} – 10^{-17} m^2 vs 10^{-18} – 10^{-13} m^2, respectively, Brace, 1980, Taillefer, 2017). Further, cross-sections of the study area (from Taillefer et al., 2017, see Supporting Information) reveal that metasediments constitute only a small part of the basement in the Têt fault footwall, from where most of the hydrothermal fluids originate. However, they could act as a layer-seal for driving fluids from depth to the surface and localizing hot spring as suggested by Taillefer et al., 2017 and Taillefer, 2017. In that sense, testing permeability contrasts related to lateral and vertical variations of the lithology in a future numerical model would be essential. The importance of the Neogene basins is more controversial: on the one hand the constitutive lithologies are porous and often related to free convection in extensive hydrothermal system (Moeck, 2014); on the other hand, their size are really reduced in the study area and they do not localize hot springs (Taillefer et al., 2017). As a first approximation, considering the basement in the model as a homogenous unit allows catching the general processes acting in this system.

(ii) The permeability is not considered as diminishing with depth. Even though most of the authors mention a decrease of the permeability with depth (Ingebritsen and Manning, 1999; Saar and Manga, 2004; Earnest and Boutt, 2014), mainly related to the increase of the confining pressure, this relation is not clearly demonstrated for crystalline and metamorphic rocks (Brace, 1980, 1984; Stober and Bucher, 2015; Ranjram et al., 2015), especially for depths greater than 500 m where data are rare and cover permeability ranges between 10^{-20} and 10^{-14} m^2. Without more information about rock permeability and its evolution with depth in the study area, testing a homogenous permeability in the model allows identifying the depths where the basement is necessarily still permeable to reproduce thermal anomalies at

the surface. Taillefer (2017) proposes, based on elastic models applied to fracture apertures in the study area, a permeability decrease that would be tested in future simulations.

(iii) The transient effects of glaciations on the hydrothermal system are not taken into account. The effects of glaciation on the groundwater recharge is still an investigated topic, because numerous processes related to the geological and glacial contexts are involved, but data sets are currently insufficient (Neuzil, 2012). Numerical studies of the transitional effects of the last glaciation on Alps hydrothermal systems use the assumption that glaciations block the groundwater recharge and that a deglaciation is necessary to reproduce the currently observed temperatures (Maréchal et al., 1999; Thiebaud, 2008; Thiebaud et al., 2010; Volpi et al., 2017), which is not our case. Further, some other studies indicate that glaciers do not suspend fluid infiltrations, except maybe if impermeable permafrost develops (Ge et al., 2008; Lemieux et al., 2008). Anyway, as discussed in the section 5.1, the ice cover during the last glaciation did not extend over the entire infiltration area (Delmas et al., 2009; Calvet et al., 2014), which at worst had blocked only a small part of the inflow probably negligible at the reservoir scale (considering the residence time). However, this could motivate a comparison of the transient effects of glaciation between Alpine and Pyrenean hydrothermal systems.

Future complex models should also incorporate other mapped secondary faults in the area (Figure 1), and test various geometries at depth as long as seismic profiles fail to precisely image the normal fault network in the basement (Diaz et al., 2018). Using the new light tomography methods adapted to sharp topography could be useful to improve the sub-surface fault geometries.

However, although our modelling approach does not take into account these elements, it allows reproducing thermal anomalies at places where hot springs are observed, with amplitudes of temperature consistent with the temperatures observed at the surface, but also those calculated at depth using geothermometers. As a first step, a simplified model is necessary to understand the primary processes influencing the hydrothermal system.

5.3 Secondary processes in fluid-rock interactions

As mentioned in Section 3.2.1, the δ^7Li ratio of the Têt hot springs is high when compared to the signature of the Dorres-Colomer hot springs (Figure 2b), and is also not in agreement with the common δ^7Li ratio of crystalline rocks. However, the deep fluid pathways in numerical models (Figure 5) suggest that the fluids circulate exclusively in crystallines rocks. Indeed, carbonates are rare and concentrated in the NE portion of the study area (Figure 1). Krimissa (1995) reached similar conclusions with respect of the $^{87}Sr/^{86}Sr$ and $^{36}Cl/Cl_{total}$ ratios, and the weak mineralization of the fluid. Thus, other processes are needed to explain why the δ^7Li ratio of the Têt hot springs is different from the crystalline bedrock. Two processes could affect the isotope fractionation during the fluid-rock interactions:

1. ^{6}Li and ^{7}Li are preferentially retained in the mineral and fluid phases, respectively. The crystallization of secondary mineral phases, e.g., clays, induces ^{6}Li depletion in the fluid, producing an increase in the δ^7Li ratio. This would be consistent with the hydrothermal alteration deposits observed in many sites around the hot springs, e.g., Thues-entre-Valls (Taillefer et al., 2017), and would support the hypothesis of the partial sealing of the Têt fault (see Section 5.2).

2. Millot et al. (2010) showed that the lithium isotope fractionation in hydrothermal fluids is inversly correlated with temperature. The cooling of the hydrothermal fluid during its transfer from depth to the surface could also increase the δ^7Li ratio.

Further, the similarities in chemical signatures between the Têt hot springs (Figure 2), already observed by Krimissa (1995), suggest that the hydrothermal fluids have the same interactions with rocks. This supports observations that the great majority of the flow lines converging toward the hot springs originate from the Têt fault's footwall or along the fault in numerical models (Figure 5c). The only exception is the Serre de Clavera range in the hanging-wall that contributes to the Canaveilles hot springs. This could explain the difference of Na and Cl concentrations of the Gr. Amont-Riviere hydrothermal fluids, and the hanging wall location of this spring cluster, with respect to the other Têt hot springs.

5.4 Conceptual model of hydrothermal flows in the Têt valley

Based on our results and those of Taillefer et al. (2017) and Taillefer (2017), we propose a conceptual model of the Têt hydrothermal system (Figure 8). Infiltration areas for the meteoric fluids are located at high elevations (above 2000 m), on the highlands constituting the Têt fault footwall. The basement is permeable down to three kilometers, allowing fluids to warm because of the regional heat flow. The circulation depth depends on the local topographic gradient, which controls the maximum fluid temperature and thus the hot spring temperatures. The Têt hydrothermal system is divided into three parts, corresponding to the main mountain ranges.

The hydrothermal fluids at the Thues-les-bains/Canaveilles and Saint-Thomas-les-bains/Prats-Balaguer hot springs come from the Carança range. The Prats fault conveys warm

fluids from the high peaks to the Saint-Thomas-les-bains/Prats-Balaguer hot spring cluster, thus compensating for the infiltration of cold fluid along the Têt fault at Planes. There, part of the fluid infiltration may become heated at depth along the Têt fault and contribute to the Thues-les-bains hot spring cluster. A Têt fault outcrop located between Thues-les-bains and Saint-Thomas-les-bains (see Taillefer et al., 2017 and Taillefer, 2017) shows that the Têt fault core zone is cataclastic (thus quite impermeable, Caine et al., 2010) and that alteration minerals here seal the entire fault zone. The hydrothermal fluids flowing at depth may be diverted below these sealed area into the adjacent hot spring clusters, i.e, Thues-les-bains and Saint-Thomas, and maybe contribute to them). Moreover, a portion of the thermal fluids is suspected of coming from the Têt fault hanging-wall to join the Canaveilles hot spring cluster, explaining its specific location in this fault compartment. The hydrothermal activity decreases on each side of this central zone along with the Têt footwall topographic gradient. The hydrothermal fluids at Llo come from the Puigmal range and possibly from the Planes infiltration area. The Vernet-les-bains hydrothermal fluid comes from the Canigou range.

The fluids coming from the moutain ranges are caught by the permeable highly fractured damage zone of the Têt fault (Taillefer et al., 2017), which leads them to the surface, explaining the close proximity of the springs and the Têt fault. The hot spring locations at the surface are more specifically related to the presence of gneiss-metasediment contacts, and the permeable mylonites of the exhumed CMNC ductile fault (see Section 2.2 and Taillefer et al., 2017).

6 Summary and conclusion

This study performs the first 3-D numerical model coupling a realistic topography and fault network that allows a better understanding of the fluid circulation and heat transfer

processes involved in the orogenic belt type hydrothermal system of the Têt fault. Both numerical models and hydrochemical data indicate that meteoric fluid infiltrations are located at high elevations (above 2000 m), on the highlands constituting the Têt fault footwall. The basement is probably permeable down to more than three kilometers, allowing fluids to become heated because of the regional heat flow. The circulation depth is governed by topography-driven forced convection, depends on the local and regional topographic gradients with respect to the faults, and is related to the maximum fluid temperature at depth and hence to the hot spring temperatures. The fluids coming from the highlands are caught by the permeable highly fractured damage zone of the Têt fault, which leads them to the surface, explaining the close proximity of the springs and the Têt fault. We therefore show that even in such context of dormant fault adjacent to high relief, the model's fluid upflows into fault damage zones allows imply clusters of hot springs with temperatures up to 73°C and geothermal gradients of 100-160°C/km close to the surface.

Combining surface structural data, hot spring temperatures and locations, and geochemical analyses with numerical models enables hydrothermal processes to be studied even in the absence of deep-level data. This study highlights the importance of considering the topography in the three dimensions and the location of the fault network with respect to the topography for the proper understanding of hydrothermal systems along dormant faults in orogenic belt contexts. Our results concerning the amplitudes and wavelengths of thermal anomalies around faults should be considered when thermochronology techniques are undertaken in such areas. Finally, since dormant faults may host such high temperatures, development of new medium-enthalpy geothermal systems could be envisaged in places not expected previously for geothermal exploration. This new and inexpensive method allows

geothermal exploration at a large scale, in mountainous regions with sharp topography, where geophysical methods or boreholes have not been operated.

Acknowledgments

This work is a part of a PhD thesis that was funded by the RGF (Référentiel Géologique de la France) project led by the French Geological Survey (BRGM, Bureau de Recherches Géologiques et Minières), which we thank for its financial and technical support. The data used in this study are included in the supporting information and are available in the PhD thesis manuscript of Taillefer (2017), downloadable at https://tel.archives-ouvertes.fr/tel-01704673/document. We thank Guy Vasseur, Jean Chéry, Severine Caritg, Béatrice Ledesert and Mathieu Bellanger, for valuable discussions. We also thank Boris Kaus, Christoph von Hagke, and an anonymous reviewer, whose constructive comments have allowed us to greatly improve the manuscript. We finally thank Gaetan Milesi, Pierre-Yves Bres, Justine Villard, and Kevin Valera for collecting data. Additional details on hot springs geochemistry, numerical procedure and geological constraints on the 3-D numerical models are given in supporting information, which also includes supplementary thermal cross-sections.

References

Allen, D. M., Grasby, S. E., and Voormeij, D. A. (2006). Determining the circulation depth of thermal springs in the southern Rocky Mountain Trench, south-eastern British Columbia, Canada using geothermometry and borehole temperature logs. *Hydrogeology Journal*, *14*(1-2), 159-172.

Autran, A., Calvet, M., and Delmas, M. (1986). Carte géologique de la france à 1/50 000, feuille Mont-Louis. *BRGM*.

Barbey, P., Cheilletz, A., and Laumonier, B. (2001). The Canigou orthogneisses (eastern Pyrenees, france, spain): an early Ordovician rapakivi granite laccolith and its contact aureole. *Comptes Rendus de l'Académie des Sciences- Series IIA-Earth and Planetary Science*, 332(2):129–136.

Belgrano, T. M., Herwegh, M., and Berger, A. (2016). Inherited structural controls on fault geometry, architecture and hydrothermal activity: an example from Grimsel Pass, Switzerland. *Swiss Journal of Geosciences*, *109(3)*,345–364.

Bense, V., Gleeson, T., Loveless, S., Bour, O., and Scibek, J. (2013). Fault zone hydrogeology. *Earth-Science Reviews*, *127*, 171–192.

Blackwell, D. D., Golan, B., and Benoit, D. (2000). Temperatures in the Dixie Valley Geothermal System. *Transactions-Geothermal Resources Council*, 223-228.

Bossong, C. R., Caine, J. S., Stannard, D. I., Flynn, J. L., Stevens, M. R., & Heiny-Dash, J. S. (2003). Hydrologic conditions and assessment of water resources in the Turkey

Creek Watershed, Jefferson County, Colorado, 1998–2001. USGS Water-Resources Investigations Report, 03-4034.

Brace, W. F. (1980). Permeability of crystalline and argillaceous rocks. In International Journal of Rock Mechanics and Mining Sciences & Geomechanics Abstracts (Vol. 17, No. 5, pp. 241-251). Pergamon.

Brace, W. (1984). Permeability of crystalline rocks : New in situ measurements. *Journal of Geophysical Research : Solid Earth*, 89(B6) :4327–4330.

Braun, J. (2002). Quantifying the effect of recent relief changes on age–elevation relationships. *Earth and Planetary Science Letters*, 200(3-4): 331-343.

Briais, A., Armijo, R., Winter, T., Tapponnier, P., and Herbecq, A. (1990). Morphological evidence for quaternary normal faulting and seismic hazard in the Eastern Pyrenees. In *Annales tectonicae*, 4: 19–42.

Cabrera, L., Roca, E., and Santanach, P. (1988). Basin formation at the end of a strike-slip fault : the Cerdanya basin (Eastern Pyrenees). *Journal of the Geological Society*, 145(2) :261–268.

Caine, J. S., A. H. Manning, P. L. Verplanck, D. J. Bove, K. G. Kahn, and S. Ge (2006), Well construction information, lithologic logs, water level data, and overview of research in Handcart Gulch, Colorado: An alpine watershed affected by metalliferous hydrothermal alteration, U.S. Geol. Surv. Open File, 06–1189.

Caine, J. S., Bruhn, R. L., and Forster, C. B. (2010). Internal structure, fault rocks, and inferences regarding deformation, fluid flow, and mineralization in the seismogenic Stillwater normal fault, Dixie Valley, Nevada. *Journal of Structural Geology*, *32*(11), 1576-1589.

Calcagno, P., Chilès, J.-P., Courrioux, G., and Guillen, A. (2008). Geological modelling from field data and geological knowledge: Part i. modelling method coupling 3d potential-field interpolation and geological rules. *Physics of the Earth and Planetary Interiors*, 171(1), 147–157.

Calvet, M. (1999). Régimes des contraintes et volumes de relief dans l'est des Pyrénées/stress regimes and volumes of reliefs in the Eastern Pyrenees. *Géomorphologie: relief, processus, environnement*, 5(3):253–278.

Calvet, M., Gunnell, Y., and Delmas, M. (2014). The Têt river valley: a condensed record of long-term landscape evolution in the Pyrenees. In *Landscapes and Landforms of France*, 127–138.

Calvet, M., Gunnell, Y., Braucher, R., Hez, G., Bourlès, D., Guillou, V., Delmas, M. (2015a). Cave levels as proxies for measuring post-orogenic uplift: Evidence from cosmogenic dating of alluvium-filled caves in the French Pyrenees. *Geomorphology*, 246 :617–633.

Carozza, J.-M. and Delcaillau, B. (2000). Réponse des bassins versants à l'activité tectonique : l'exemple de la terminaison orientale de la chaîne Pyrénéenne. Approche morphotectonique/drainage basins response to active tectonics : example from Eastern Pyrenees. morphotectonic approach. *Géomorphologie : relief, processus, environnement*, 6(1) :45–60.

Carozza, J.-M. and Baize, S. (2004). L'escarpement de faille de la Têt est-il le résultat de la tectonique active plio-pléistocène ou d'une exhumation pléistocène ? *Comptes Rendus Géoscience*, 336(3) :217–226.

Choukroune, P., Seguret, M., and Galdeano, A. (1973). Caracteristiques et evolution structurale des Pyrenees ; un modele de relations entre zone orogenique et mouvement des plaques. *Bulletin de la Société géologique de France*, 7(5-6) :600–611.

Clauser, C. (1992). Permeability of crystalline rocks. Eos, Transactions American Geophysical Union, 73(21), 233-238.

Courtois N., Le Strat P., avec la collaboration de P. Vigouroux (2004) - Valorisation de la ressource en eau chaude et développement local du Canton d'Olette (66). BRGM/RP-53078- FR, 153 p., 62 ill., 5 ann.

Cox, S. C., Menzies, C. D., Sutherland, R., Denys, P. H., Chamberlain, C., and Teagle, D. A. (2015). Changes in hot spring temperature and hydrogeology of the alpine fault hanging wall, new zealand, induced by distal south island earthquakes. *Geofluids*, 15(1- 2) :216–239.

Craw, D., Koons, P., Zeitler, P., and Kidd, W. (2005). Fluid evolution and thermal structure in the rapidly exhuming gneiss complex of Namche Barwagyala Peri, eastern Himalayan syntaxis. *Journal of Metamorphic Geology*, 23(9) :829–845.

Craw, D., Upton, P., Horton, T., and Williams, J. (2013). Migration of hydrothermal systems in an evolving collisional orogen, New Zealand. *Mineralium Deposita*, *48*(2), 233-248.

Curewitz, D. and Karson, J. A. (1997). Structural settings of hydrothermal outflow: Fracture permeability maintained by fault propagation and interaction. *Journal of Volcanology and Geothermal Research*, *79(3)*,149–168.

Delcaillau, B., Carozza, J.-M., and Font, M. (2004). Le segment nord de la faille de la Têt (Pyrénées-Orientales): fonctionnement néogène et implications géomorphologiques. *Bulletin Société Géologique de France*, (3):257–272.

Delmas, M., Calvet, M., and Gunnell, Y. (2009). Variability of quaternary glacial erosion rates–a global perspective with special reference to the eastern Pyrenees. *Quaternary Science Reviews*, 28(5) :484–498.

Diaz, J., Vergés, J., Chevrot, S., Antonio-Vigil, A., Ruiz, M., Sylvander, M., & Gallart, J. (2018). Mapping the crustal structure beneath the Eastern Pyrenees. Tectonophysics, 744, 296-309.

Earnest, E. and Boutt, D. (2014). Investigating the role of hydromechanical coupling on flow and transport in shallow fractured-rock aquifers. *Hydrogeology journal*, 22(7) :1573–1591.

Ehlers, T. A. and Chapman, D. S. (1999). Normal fault thermal regimes: conductive and hydrothermal heat transfer surrounding the Wasatch fault, Utah. *Tectonophysics*, 312(2):217–234.

Ellis, A. (1970). Quantitative interpretation of chemical characteristics of hydrothermal systems. *Geothermics*, 2:516–528.

Evans, J. P., Forster, C. B., & Goddard, J. V. (1997). Permeability of fault-related rocks, and implications for hydraulic structure of fault zones. Journal of structural Geology, 19(11), 1393-1404.

Faulds, J., Coolbaugh, M., Bouchot, V., Moek, I., and Oguz, K. (2010). Characterizing structural controls of geothermal reservoirs in the Great Basin, Usa, and Western Turkey: Developing successful exploration strategies in extended terranes. In *World Geothermal Congress 2010*, pages 11.

Forster, C. and Smith, L. (1988). Groundwater flow systems in mountainous terrain: 2. Controlling factors. *Water Resources Research*, *24*(7), 1011-1023.

Forster, C. and Smith, L. (1989). The influence of groundwater flow on thermal regimes in mountainous terrain: a model study. *Journal of Geophysical Research: Solid Earth*, 94(B7):9439–9451.

Fouillac, C. and Michard, G. (1981). Sodium/lithium ratio in water applied to geothermometry of geothermal reservoirs. *Geothermics*, 10(1):55–70.

Fournier, R. (1977). Chemical geothermometers and mixing models for geothermal systems. *Geothermics*, 5(1-4):41–50.

Freeze, R. A., and J. A. Cherry (1979), Groundwater, 604 pp., *Prentice-Hall*, Englewood Cliffs, N. J.

Garibaldi, C., Guillou-Frottier, L., Lardeaux, J. M., Bonté, D., Lopez, S., Bouchot, V., and Ledru, P. (2010). Thermal anomalies and geological structures in the Provence basin: Implications for hydrothermal circulations at depth. *Bulletin de la Société Géologique de France*, *181*(4), 363-376.

Ge, S., Wu, Q. B., Lu, N., Jiang, G. L., & Ball, L. (2008). Groundwater in the Tibet Plateau, western China. *Geophysical Research Letters*, 35(18).

Genti, M. (2015). Impact des processus de surface sur la déformation actuelle des Pyrénées et des Alpes. PhD thesis, Université de Montpellier.

Gleeson, T., and Manning, A. H. (2008). Regional groundwater flow in mountainous terrain: Three dimensional simulations of topographic and hydrogeologic controls. *Water Resources Research*, 44(10).

Gleeson, T., Smith, L., Moosdorf, N., Hartmann, J., Dürr, H. H., Manning, A. H., ... & Jellinek, A. M. (2011). Mapping permeability over the surface of the Earth. Geophysical Research Letters, 38(2).

Glotzbach, C., Spiegel, C., Reinecker, J., Rahn, M., and Frisch, W. (2009). What perturbs isotherms? an assessment using fission-track thermochronology and thermal

modelling along the Gotthard transect, Central Alps. *Geological Society, London, Special Publications*, 324(1):111–124.

Goula, X., Olivera, C., Fleta, J., Grellet, B., Lindo, R., Rivera, L., Cisternas, A., and Carbon, D. (1999). Present and recent stress regime in the eastern part of the Pyrenees. *Tectonophysics*, 308(4):487–502.

Grasby, S. E. and Hutcheon, I. (2001). Controls on the distribution of thermal springs in the southern canadian cordillera. *Canadian Journal of Earth Sciences*, 38(3) :427–440.

Guillou-Frottier, L., Carre˙, C., Bourgine, B., Bouchot, V., and Genter, A. (2013). Structure of hydrothermal convection in the Upper Rhine graben as inferred from corrected temperature data and basin-scale numerical models. *Journal of Volcanology and Geothermal Research*, 256:29–49.

Guitard, G., Geyssant, J., Laumonier, B., Autran, A., Fonteilles, M., Dalmayrac, B., Vidal, J., and Bandet, Y. (1992). Carte géol. france (1/50 000), feuille prades (1095). *BRGM, Orléans*.

Guitard, G., Laumonier, B., Autran, A., Bandet, Y., and Berger, G. (1998). Notice explicative, carte géologique france (1: 50.000), feuille prades (1095). *BRGM, Orléans*. Hoefs, J. and Sywall, M. (1997). Lithium isotope composition of quaternary and tertiary biogene carbonates and a global lithium isotope balance. *Geochimica et Cosmochimica Acta*, 61(13):2679–2690.

Howald, T., Person, M., Campbell, A., Lueth, V., Hofstra, A., Sweetkind, D., Gable C. W., Banerjee, A., Luijendijk, E., Crossey, L., Karlstrom, K., Kelley, S., Phillips, F.M. (2015). Evidence for long timescale (> 103 years) changes in hydrothermal activity induced by seismic events. *Geofluids*, *15*(1-2), 252-268.

Hubbert, M. K. (1940). The theory of groundwater motion. *The Journal of Geology*, 48(8, Part 1) :785–944.

Ingebritsen, S. and Manning, C. E. (1999). Geological implications of a permeability-depth curve for the continental crust. *Geology*, 27(12) :1107–1110.

Ingebritsen, S. E. and Gleeson, T. (2015). Crustal permeability: Introduction to the special issue. *Geofluids*, 15(1-2):1–10.

Jarman, D., Calvet, M., Corominas, J., Delmas, M., and Gunnell, Y. (2014). Large scale rock slope failures in the eastern Pyrenees: identifying a sparse but significant population in paraglacial and parafluvial contexts. *Geografiska Annaler: Series A, Physical Geography*, *96*(3), 357-391.

Jaupart, C. (1983). Horizontal heat transfer due to radioactivity contrasts: causes and consequences of the linear heat flow relation. *Geophysical Journal International*, *75*(2), 411-435.

Krimissa, M. (1995). Application des méthodes isotopiques à l'étude des eaux thermales en milieu granitique (Pyrénées, France). PhD Thesis, Université Paris XI.

Lacan, P. (2012). Active tectonics of the Pyrenees: A review/revisión de la tectónica activa de los pirineos. *Journal of Iberian Geology*, 38(1):9–30.

Ladouche B., Lamotte C. Le-Goff E., Vigouroux P. (2014) – Etat des lieux ressource en eau thermale du site des Escaldes (66). Rapport final BRGM/RP-63985-FR, 98 p., 30 ill., 6 ann.

Lapwood, E. (1948). Convection of a fluid in a porous medium. *Mathematical Proceedings of the Cambridge Philosophical Society*, Vol. 44, pp. 508–521.

Lemieux, J. M., Sudicky, E. A., Peltier, W. R., & Tarasov, L. (2008). Dynamics of groundwater recharge and seepage over the Canadian landscape during the Wisconsinian glaciation. *Journal of Geophysical Research: Earth Surface*, 113(F1).

Lewis, C. J., Vergés, J., and Marzo, M. (2000). High mountains in a zone of extended crust: Insights into the neogene-quaternary topographic development of northeastern Iberia. *Tectonics*, 19(1):86–102.

López, D. L., and Smith, L. (1995). Fluid flow in fault zones: analysis of the interplay of convective circulation and topographically driven groundwater flow. *Water Resources Research*, 31(6):1489–1503.

Lowell, R. P., Van Cappellen, P., and Germanovich, L. N. (1993). Silica precipitation in fractures and the evolution of permeability in hydrothermal upflow zones. *Science*, 260, 192–194.

Lucazeau, F. and Vasseur, G. (1989). Heat flow density data from France and surrounding margins. *Tectonophysics, 164(2-4),*251–258.

Magri, F., Inbar, N., Siebert, C., Rosenthal, E., Guttman, J., and Möller, P. (2015). Transient simulations of large-scale hydrogeological processes causing temperature and salinity anomalies in the Tiberias basin. *Journal of Hydrology, 520*, 342–355.

Magri, F., Möller, S., Inbar, N., Möller, P., Raggad, M., Rödiger, T., Rosenthal, E., and Siebert, C. (2016). 2d and 3d coexisting modes of thermal convection in fractured hydrothermal systems-implications for transboundary flow in the lower Yarmouk gorge. *Marine and Petroleum Geology*, 78:750–758.

Malkovsky, V., and Pek, A. (2004). Timescales for reaching steady-state fluid flow in systems perturbed by formation of highly permeable faults. *Geofluids, 4(4),* 253–258.

Malkovsky, V. I., and Magri, F. (2016). Thermal convection of temperature-dependent viscous fluids within three-dimensional faulted geothermal systems: Estimation from linear and numerical analyses. *Water Resources Research*, 52(4):2855–2867.

Malavieille, J., and Konstantinovskaya, E. (2010). Impact of surface processes on the growth of orogenic wedges: insights from analog models and case studies. *Geotectonics, 44*(6), 541-558.

Maréchal, J. C., Perrochet, P., & Tacher, L. (1999). Long-term simulations of thermal and hydraulic characteristics in a mountain massif: The Mont Blanc case study, French and Italian Alps. *Hydrogeology Journal*, 7(4), 341-354.

Mauffret, A., de Grossouvre, B. D., Dos Reis, A. T., Gorini, C., and Nercessian, A. (2001). Structural geometry in the eastern Pyrenees and western Gulf of Lion (western Mediterranean). *Journal of Structural Geology*, 23(11):1701– 1726.

Maurel, O. (2003). L'exhumation de la Zone Axiale des Pyrénées orientales: Une approche thermo-chronologique multi-méthodes du rôle des failles. PhD thesis, Université Montpellier II.

Maurel, O., Monnier, P., Pik, R., Arnaud, N., Brunel, M., and Jolivet, M. (2008). The meso-cenozoic thermo-tectonic evolution of the eastern Pyrenees: an 40 ar/39 ar fission track and (u–th)/he thermochronological study of the Canigou and Mont-Louis massifs. *International Journal of Earth Sciences*, 97(3):565–584.

McKenna, J. R., and Blackwell, D. D. (2004). Numerical modeling of transient Basin and Range extensional geothermal systems. *Geothermics, 33(4),* 457– 476.

Millot, R., and Négrel, P. (2007). Multi-isotopic tracing (δ7Li, δ11B, 87Sr/86Sr) and chemical geothermometry: evidence from hydro-geothermal systems in France. *Chemical Geology, 244(3),* 664–678.

Millot, R., Négrel, P., and Petelet-Giraud, E. (2007). Multi-isotopic (Li, B, Sr, Nd) approach for geothermal reservoir characterization in the limagne basin (massif central, france). *Applied Geochemistry, 22(11),*2307–2325.

Millot, R., Petelet-Giraud, E., Guerrot, C., and Négrel, P. (2010). Multi-isotopic composition (δ7Li, δ11B, δD–δ18O) of rainwaters in France: origin and spatio-temporal characterization. *Applied Geochemistry*, *25(10)*, 1510–1524.

Moeck, I. S. (2014). Catalog of geothermal play types based on geologic controls. *Renewable and Sustainable Energy Reviews*, 37:867– 882.

Négrel, P., Guerrot, C., and Millot, R. (2007). Chemical and strontium isotope characterization of rainwater in France: influence of sources and hydrogeochemical implications. *Isotopes in Environmental and Health Studies*, *43(3)*:179–196.

Neuzil, C. E. (2012). Hydromechanical effects of continental glaciation on groundwater systems. *Geofluids*, 12(1), 22-37.

Padel, M. (2016). Influence cadomienne dans les séries pré-sardes des Pyrénées Orientales: approche géochimique, stratigraphique et géochronologique. PhD thesis, Lille 1.

Person, M., Hofstra, A., Sweetkind, D., Stone, W., Cohen, D., Gable, C., and Banerjee, A. (2012). Analytical and numerical models of hydrothermal fluid flow at fault intersections. *Geofluids*, *12(4)*, 312–326.

Petit, C. and Mouthereau, F. (2012). Steep topographic slope preservation by anisotropic difusion: An example from the Neogene Têt fault scarp, Eastern Pyrenees. *Geomorphology*, 171 :173–179.

Petit V., Le Goff E. avec la collaboration de N. Brisset (2010) - Ressource en eau thermale des Thermes de Vernet-Les-Bains – État des lieux (Pyrénées Orientales). BRGM/RP-59182-FR, 73 p., 20 ill., 5 ann.

Philip, H., Bousquet, J.-C., Escuer, J., Fleta, J., Goula, X., and Grellet, B. (1992). Présence de failles inverses d'âge quaternaire dans l'est des Pyrénées: implications sismotectoniques. *Comptes rendus de l'Académie des sciences. Série 2, Mécanique, Physique, Chimie, Sciences de l'univers, Sciences de la Terre*, 314(11):1239–1245.

Rabinowicz, M., Boulègue, J., and Genthon, P. (1998). Two-and three-dimensional modeling of hydrothermal convection in the sedimented Middle Valley segment, Juan de Fuca ridge. *Journal of Geophysical Research : Solid Earth*, 103(B10) :24045–24065.

Ranjram, M., Gleeson, T., and Luijendijk, E. (2015). Is the permeability of crystalline rock in the shallow crust related to depth, lithology or tectonic setting ? *Geofluids*, 15(1-2):106–119.

Renard, F., Gratier, J.-P., and Jamtveit, B. (2000). Kinetics of crack-sealing, intergranular pressure solution, and compaction around active faults. *Journal of Structural Geology, 22(10)*, 1395–1407.

Roche, V., Sternai, P., Guillou-Frottier, L., Menant, A., Jolivet, L., Bouchot, V., and Gerya, T. (2018). Emplacement of metamorphic core complexes and associated geothermal systems controlled by slab dynamics. *Earth and Planetary Science Letters, 498*, 322-333.

Roure, F., Choukroune, P., Berastegui, X., Mu- noz, J., Villien, A., Matheron, P., Bareyt, M., Seguret, M., Camara, P., and Deramond, J. (1989). Ecors deep seismic data and ba- lanced cross sections : Geometric constraints on the evolution of the Pyrenees. *Tectonics*, 8(1):41–50.

Saar, M. and Manga, M. (2004). Depth dependence of permeability in the Oregon cascades inferred from hydrogeologic, thermal, seismic, and magmatic modeling constraints. *Journal of Geophysical Research : Solid Earth*, 109(B4).

Saffer, D., M., Bekins, B. A., and Hickman, S. (2003). Topographically driven groundwater flow and the San Andreas heat flow paradox revisited. *Journal of Geophysical Research : Solid Earth*, *108*(B5).2274.

Sartégou A., Bourlès D. L., Blard P. H., Braucher R., Tibari B., Zimmermann L., Leanni L., Aumaître G., Keddadouche K., (2018). Deciphering landscape evolution with karstic networks: A Pyrenean case study. *Quaternary Geochronology*, *43*:12-29.

Saula, E., Picart, J., Mató, E., Llenas, M., Losantos, M., Berástegui, X., and Agustí, J. (1994). Evolución geodinámica de la fosa del Empordà y las Sierras Transversales. *Acta geológica hispánica*, 29(2-4):55–75.

Séranne, M. (1999). The Gulf of Lion continental margin (NW Mediterranean) revisited by ibs : an overview. *Geological Society, London, Special Publications*, 156(1):15–36.

Sonney, R. and Vuataz, F.-D. (2009). Numerical modelling of alpine deep flow systems: a management and prediction tool for an exploited geothermal reservoir (Lavey-les-bains, Switzerland). *Hydrogeology Journal*, 17(3):601– 616.

Souriau, A., and Pauchet, H. (1998). A new synthesis of pyrenean seismicity and its tectonic implications. *Tectonophysics, 290(3),* 221–244.

Stober, I., and Bucher, K. (1999). Deep groundwater in the crystalline basement of the Black Forest region. *Applied Geochemistry, 14(2),* 237–254.

Stober, I., and Bucher, K. (2015). Hydraulic conductivity of fractured upper crust: insights from hydraulic tests in boreholes and fluid-rock interaction in crystalline basement rocks. *Geofluids, 15(1-2),* 161–178.

Stüwe, K., White, L., and Brown, R. (1994). The influence of eroding topography on steady-state isotherms. Application to fission track analysis. *Earth and Planetary Science Letters*, *124*(1-4), 63-74.

Stüwe, K., and Hintermüller, M. (2000). Topography and isotherms revisited: The influence of laterally migrating drainage divides. *Earth and Planetary Science Letters*, *184*(1), 287-303.

Sutherland, R., Townend, J., Toy, V., Upton, P., Coussens, J., Allen, M., and Boles, A. (2017). Extreme hydrothermal conditions at an active plate-bounding fault. *Nature, 546,* 137-140.

Taillefer, A., Soliva, R., Guillou-frottier, L., Le Goff, E., Martin, G., and Seranne, M. (2017). Fault-related controls on upward hydrothermal flow; an integrated geological study of the Têt fault, eastern Pyrénées (France). *Geofluids*, vol. 2017, Article ID 8190109, 19 pages, 2017.

Taillefer, A. (2017) Interactions entre tectonique et hydrothermalisme : rôle de la faille normale de la Têt sur la circulation hydrothermale et la distribution des sources thermales de Pyrénées Orientales. PhD thesis, Université de Montpellier.

Tassone, A. A., Roca, E., Muñoz, J., Cabrera, L., and Artigas, M. C. (1994). Evolución del sector septentrional del margen continental Catalán durante el Cenozoico. *Acta geológica hispánica*, 29(2):3–37.

Thiébaud, E. (2008). Fonctionnement d'un système hydrothermal associé à un contact tectonique alpin (La Léchère, Savoie). Apports de l'hydrogéologie, de la géochimie et de la modélisation hydrodynamique et thermique en vue de la gestion de la ressource. PhD thesis, Université de Savoie.

Thiebaud, E., Gallino, S., Dzikowski, M., & Gasquet, D. (2010). The influence of glaciations on the dynamics of mountain hydrothermal systems: numerical modeling of the La Léchère system (Savoie, France). *Bulletin de la Société Géologique de France*, 181(4), 295-304.)

Tiedeman, C. R., D. J. Goode, and P. A. Hsieh (1998), Characterizing a ground water basin in a New England mountain and valley terrain, Ground Water, 36, 611–620, doi:10.1111/j.1745-6584.1998.tb02835.x.

Vernant, P., Hivert, F., Chery, J., Steer, P., Cattin, R., and Rigo, A. (2013). Erosion-induced isostatic rebound triggers extension in low convergent mountain ranges. *Geology*, 41(4):467–470.

Volpi, G., Magri, F., Frattini, P., Crosta, G. B., and Riva, F. (2017). Groundwater-driven temperature changes at thermal springs in response to recent glaciation: Bormio hydrothermal system, Central Italian Alps. *Hydrogeology Journal*, *25(7)*, 1967-1984.

White, D. E. (1965). Saline waters of sedimentary rocks. *Fluids in the Subsurface Environment*, Addison Young, John E. Galley. American Association of Petroleum Geologists, *4*:342–365.

Table 1 – Model parameters. *See section 4.1.1, **See Table 2.

Fluid properties			
Dynamic viscosity	μ	f(T) *	Pa.s
Mass density	ρ_f	f(T) *	$k.m^{-3}$
Thermal capacity	Cp_f	4180	$J.kg^{-1}.K^{-1}$
Thermal conductivity	λ_f	0.6	$W.m^{-1}.K^{-1}$
Thermal expansion coefficient	α	10^{-4}	K^{-1}
Rock properties			
Permeability	k	variable **	m^2
Mass density	ρ_s	2650	$kg.m^{-3}$
Porosity	ϕ	0.1	
Thermal capacity	Cp_s	1000	$J.kg^{-1}.K^{-1}$
Thermal conductivity	λ_s	2.5	$W.m^{-1}.K^{-1}$
Thermal expansion coefficient	β	$7\ 10^{-6}$	K^{-1}

Table 2 – Permeability values for the basement and the fault network computed for the various simulations.

	k_b (m^2)	k_{fT} (m^2)	k_{fPy}, k_{fPr} (m^2)
Simulation 1	10^{-16}	10^{-16}	-
Simulation 2	10^{-16}, 10^{-17}	10^{-16}, 10^{-15}, 5 10^{-15}, 10^{-14}	-
Simulation 3	10^{-16}	5 10^{-15}	5 10^{-15}

Table 3 – Flow-line features associated with the thermal anomalies observed during Simulation 2 (k_b=10^{-10} m^2 and k_{fT} =10^{-10} m^2).

	Maximum depth (m)	Maximum temperature (°C)	Altitude of origin (m)	Range of origin
Llo	-150	80	2600	Puigmal
St-Thomas/Prats-B.	-600	120	2650	Pic d'Eyne
Thues hanging wall	-1950	170	1750	Serre de Clavera
Thues footwall	-1300 to -3700	140 to 210	2600	Pic de la Dona / Pic d'Eyne
Vernet-les-bains	-1400	130	2450	Canigou

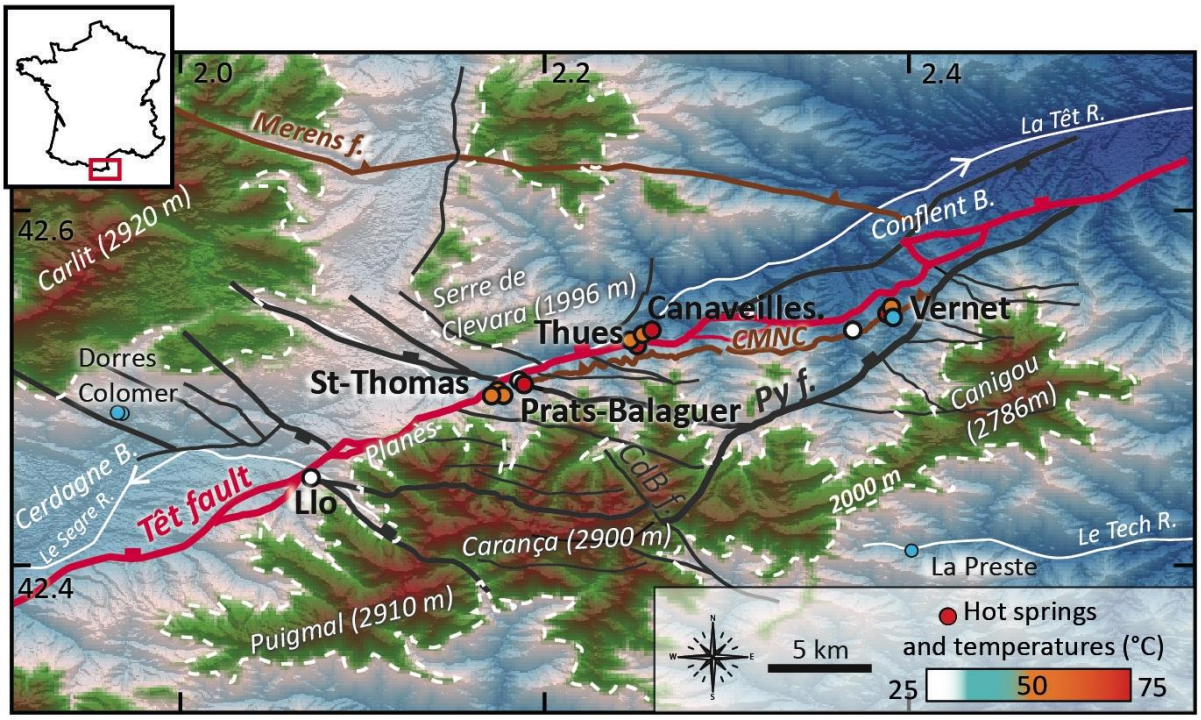

Figure 1 - Structural map of the study area showing the principal rivers (white lines), the Têt fault (red line, mostly Oligo-Miocene), the ductile faults (brown lines, mostly Hercynian), the principal subsidiary faults (grey lines, undetermined ages and sometimes kinematics), the main mountain ranges with the highest peak altitudes, the hot spring clusters with their temperatures, and the potential infiltration areas for hydrothermal fluids as determined by Krimissa [1995] (dashed lines). R: River - B: Basin - f.: fault - CdB f: Coum de Bassibes fault – CMNC : "Chevauchement Mylonitique Nord Canigou" (North Canigou Mylonitic thrust).

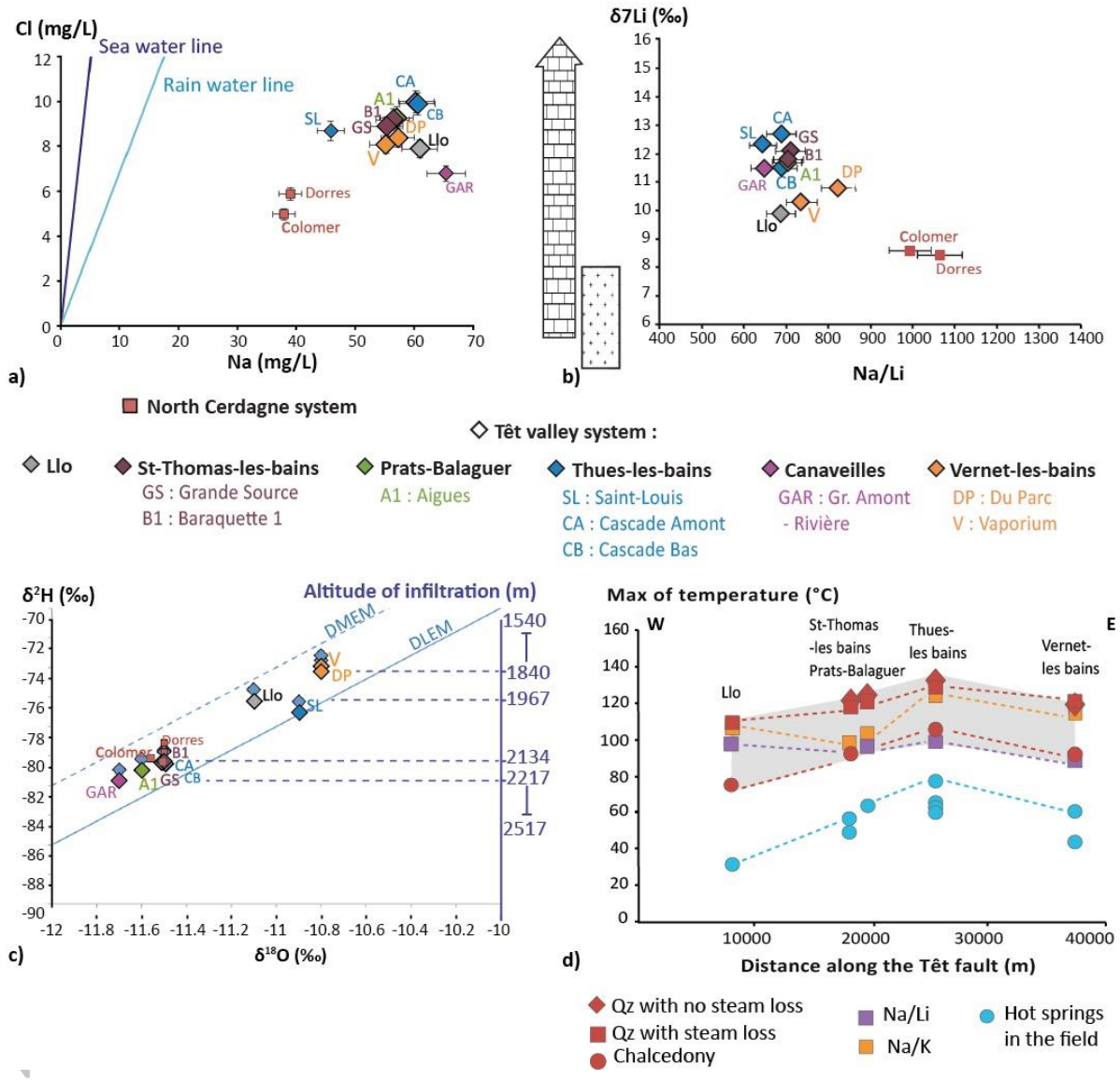

Figure 2 – Geochemical features of the Têt hot springs. The North Cerdagne system of Dorres-Colomer is indicated for comparison (Ladouche et al., 2014). The central legend is common to a, b and c. a) Na concentration as a function of Cl concentration and comparison with the sea and rain water lines; b) Lithium isotopic ratio as a function of the Na/Li concentration ratio. The typical isotopic ratios of crystalline rocks and carbonates are indicated on the left; c) Stable isotopic ratio of water (left axis) and related altitudes of infiltration (right axis) calculated from the altitude gradient established by Krimissa (1995) (with the maximum error bar of 300 m). The word (DMEM) and local (DLEM, after Négrel et al., 2007) meteoric-water lines are indicated; d) Temperature profile along the Têt fault showing the maximum of temperatures calculated from five geothermometers. Hot spring temperatures at the surface are also plotted.

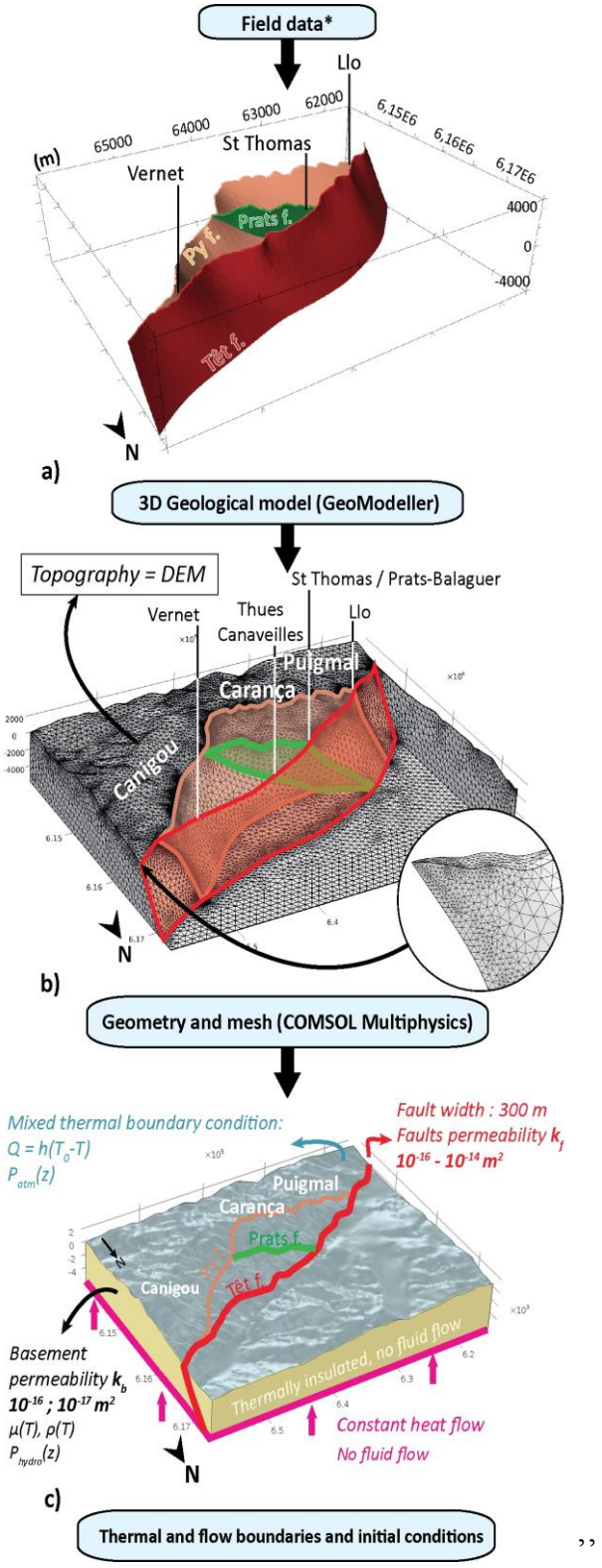

Figure 3 – Numerical method, using field data (Taillefer et al., 2017) to obtain the thermal flow model: a) The 3-D geological model with the faults considered in the simplified model (see text); b) Model mesh grid (503976 elements) refined around the fault planes (see zoom) and near the surface topography; c) Thermal and flow conditions applied to the model.

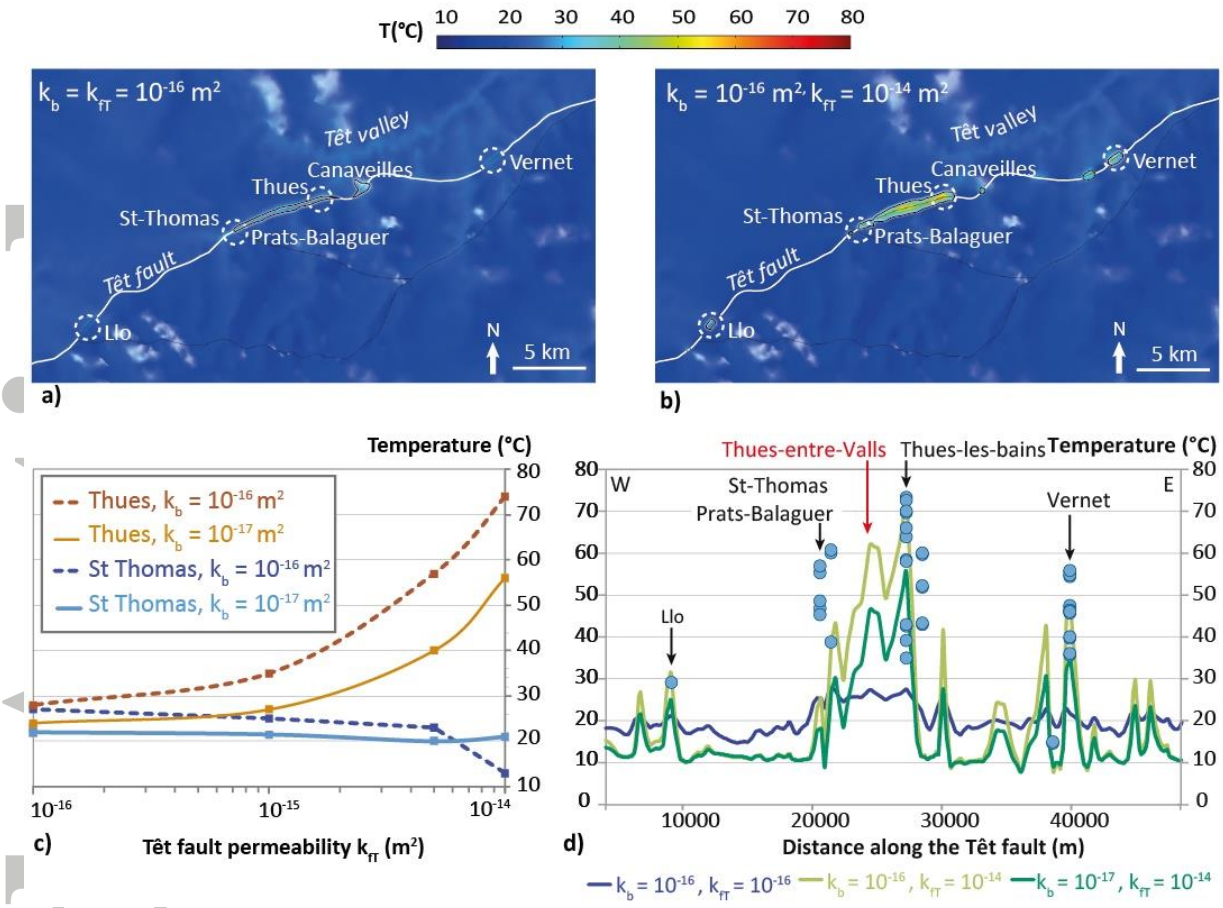

Figure 4 –Sensibility study of the effects of the Têt fault and basement permeabilities on surface temperatures. a) Model map view of the temperatures at the surface for the case with no fault or with a sealed fault; b) With a permeable fault and a relatively permeable basement; c) Temperatures at Thues and St-Thomas-les-bains as a function of the Têt fault and basement permeabilities, k_{fT} and k_b, respectively; d) Surface temperatures along the Têt fault for a sealed fault (blue), and a permeable fault with a permeable (light green) or impermeable (dark green) basement. Observed hot spring temperatures are also plotted (blue dots).

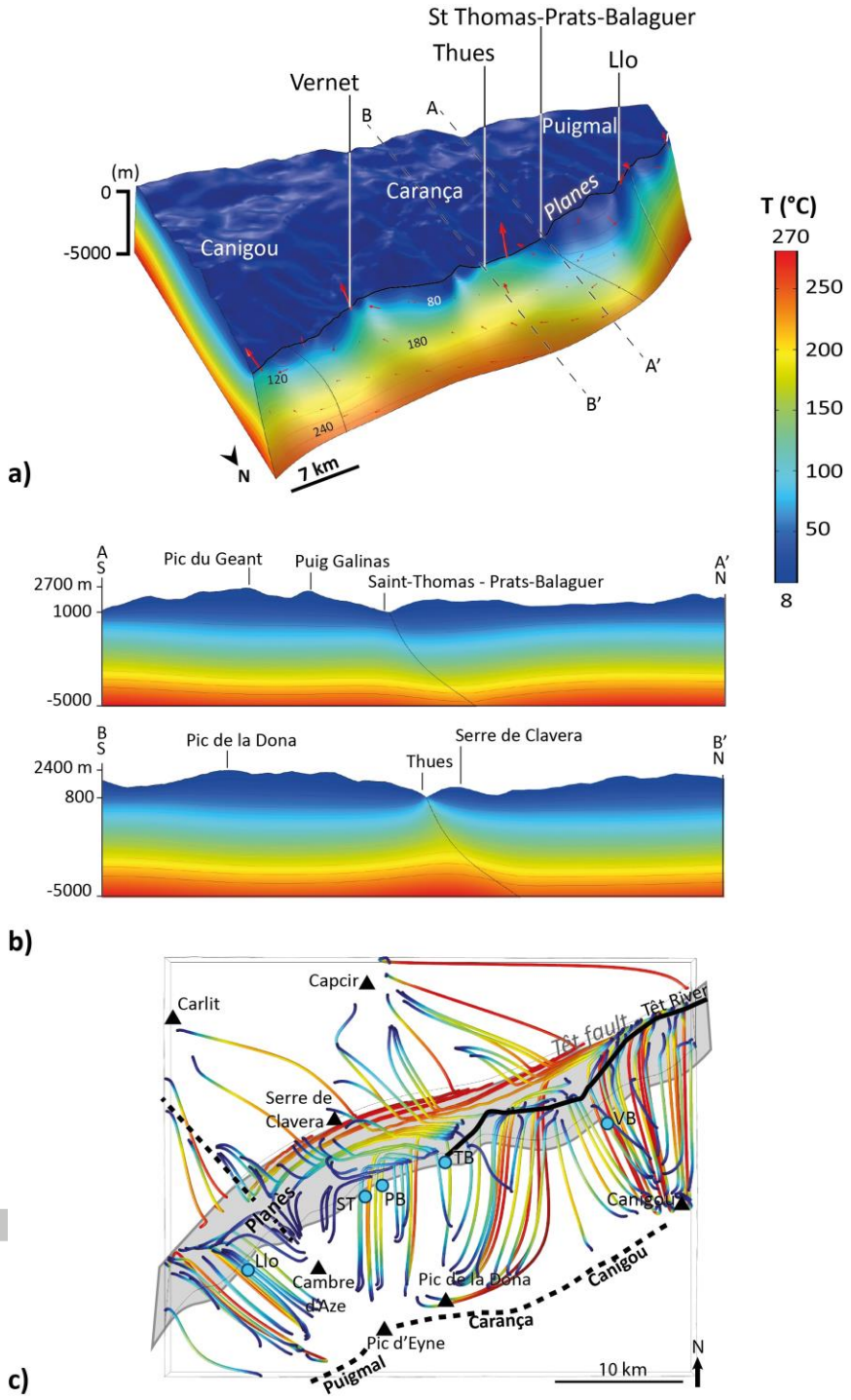

Figure 5 –Distribution of thermal anomalies at depth for the single-fault model with $k_b=10^{-16}$ m² and $k_{fT}=10^{-14}$ m². The temperature scale at right applies to all the figures. a) Thermal anomalies at depth along the Têt fault plane. The red arrows represent the Darcy velocity (the maximum value west of Thues is $1.7x10^{-8}$ m.s^{-1}). Also shown: hot spring locations, principal mountain ranges and the Planes topographic-high; b) N-S cross-sections whose lines are indicated in (a), at St- Thomas-les-bains/Prats-Balaguer (AA') and Thues-les-bains (BB'); c) Vertical view, with the hot spring locations, of the flow lines inside the model colored according to the temperature. The principal peaks and the Têt fault and river are indicated.

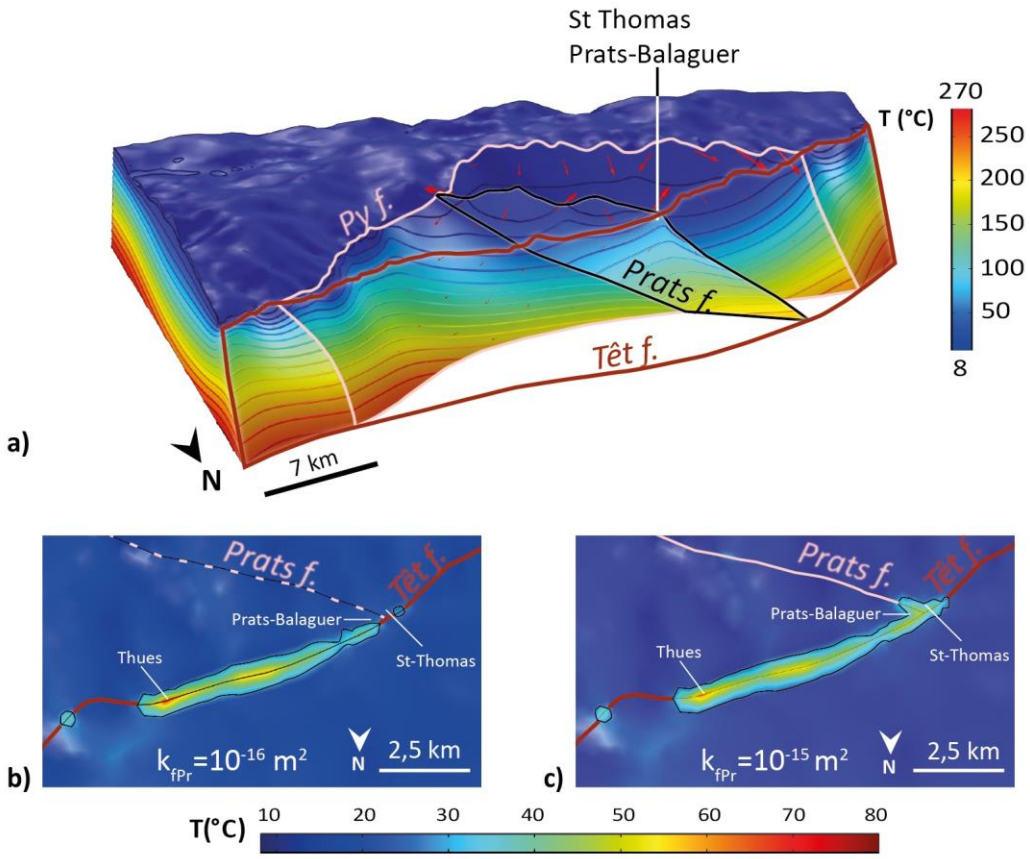

Figure 6 –Multi-fault model, with a high permeability for the Py and Prats faults (Simulation 3, Cases a) and c)), and the case of a uni-fault model (Simulation 2, Case b). a) View from the NE to the temperature along the Py and Prats faults. The red arrows represent the Darcy velocity (maximum 1.7x10−8 m.s^{-1}). b) Elarged map view of Thues and Saint-Thomas in the single-fault model (Simulation 2, see section 4.2.2). c) Enlarged map view of Thues and Saint-Thomas in the multi-fault model (Simulation 3), for comparison with (b).

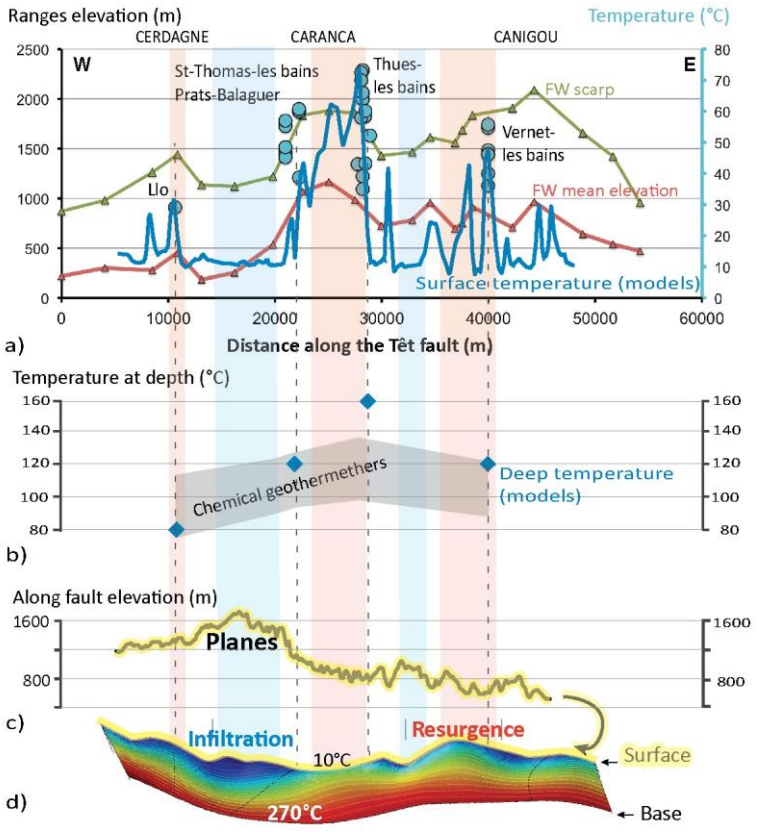

Figure 7 –Comparison of the results along the Têt fault of the combined multi-approach from Taillefer et al. (2017) and this study a) 2-D geomorphological analysis modified from Taillefer et al. (2017) showing the footwall (FW) scarp height (green line), the average of normalized altitude of the footwall integrated to its width (red line), and the hot spring temperatures (blue circle). Thermal anomalies at the surface in numerical models (from Figure 4d) are also plotted (blue line); b) Maximum temperatures given by the chemical geothermometers (grey surface from Figure 2d) and the numerical models (for $k_b=10^{-16}$ m^2 and $k_{fT}=10^{-14}$ m^2, blue diamonds); c) Topographic profile along the Têt fault; d) Isotherms distribution along the Têt fault plane in numerical models. Light blue and orange vertical shadings indicate zones of infiltration and resurgence respectively.

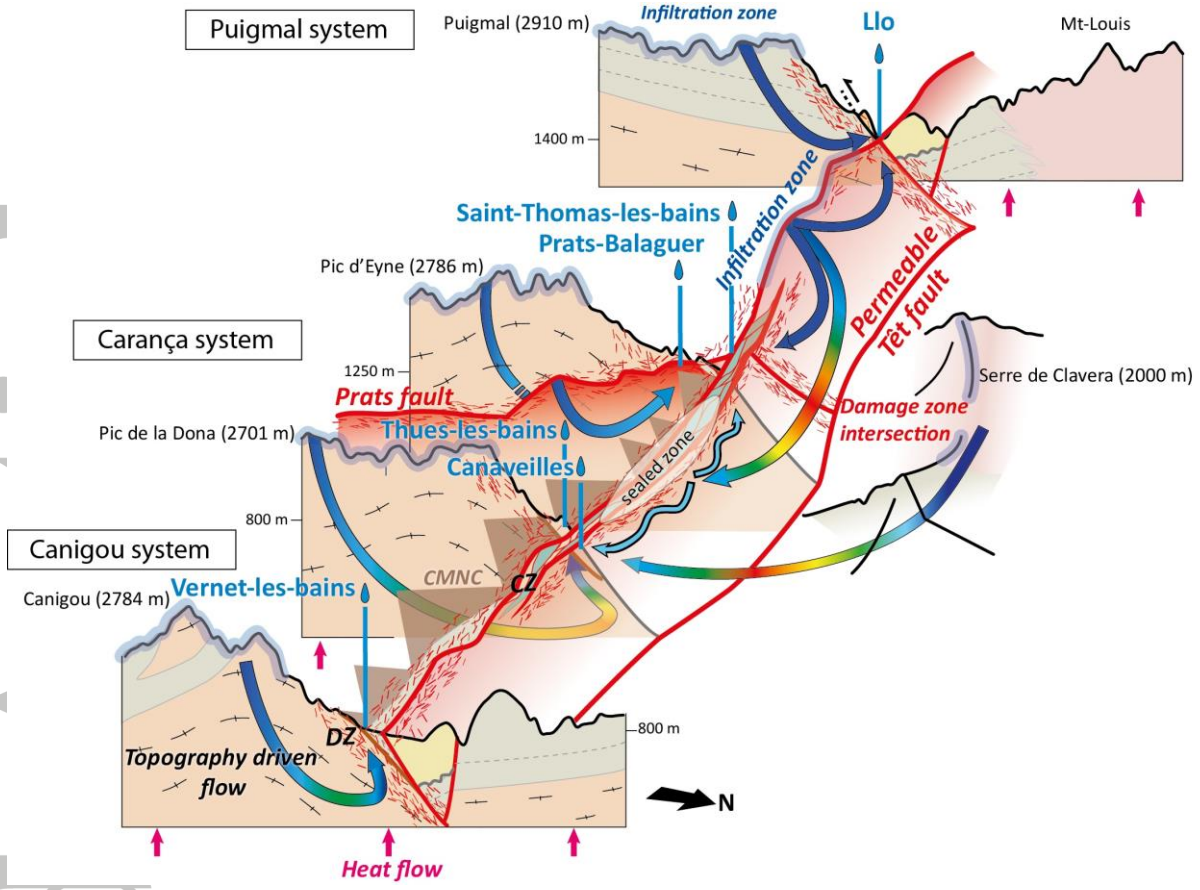

Figure 8 – Conceptual model of the Têt hydrothermal system from Taillefer et al. (2017), Taillefer (2017) and this study.